Optimization of a Pyrimidinone Series for Selective Inhibition of Ca^{2+}/Calmodulin-Stimulated Adenylyl Cyclase 1 Activity for the Treatment of Chronic Pain

Jason A. Scott[1], Monica Soto-Velasquez[1], Michael P. Hayes[1], Justin E. LaVigne[1], Heath R. Miller[1], Jatinder Kaur[1], Karin F.K. Ejendal[1], Val J. Watts[1,2,3,], Daniel P. Flaherty[1,2,3,]**

[1] Department of Medicinal Chemistry and Molecular Pharmacology, College of Pharmacy, Purdue University, West Lafayette, IN 47907, United States.

[2] Purdue Institute for Drug Discovery, West Lafayette, Indiana 47907, United States.

[3] Purdue Institute for Integrative Neuroscience, 207 South Martin Jischke Dr. West Lafayette, IN 47907, United States.

KEYWORDS: Adenylyl cyclase 1, adenylyl cyclase 8, chronic pain, drug discovery.

ABSTRACT

Adenylyl cyclase type 1 is an emerging target for the treatment of chronic pain that is downstream on the analgesic pathway from the traditional μ-opioid receptor. AC1 is expressed in the central nervous system and critical for signaling in pain sensitization. Behavioral studies have revealed AC1 knockout mice exhibit reduced behavioral pain sensitization responses similar to morphine administration. AC1, and a closely related isoform AC8, are also implicated to have a role in learning and memory signaling processes. However, reports suggest selectively targeting AC1 over AC8 may be a viable strategy to eliminate potential deleterious effects on learning and memory. Our team has carried out cellular screening for inhibitors of AC1 that yielded a pyrazolyl-pyrimidinone scaffold with potency comparable to previously published AC1 inhibitors, selectivity versus AC8, and improved drug-like physicochemical properties. Structure-activity relationship (SAR) studies produced 36 analogs that balanced improvements in potency with cellular IC_{50} values as low as 0.25 μM and selectivity versus AC8. Prioritized analogs were selective for AC1 compared to other AC isoforms and other common neurological targets. A representative analog was assessed for efficacy in a mouse model of inflammatory pain and displayed modest anti-allodynic effects. This series of compounds represents the most potent and selective inhibitors of Ca^{2+}/Calmodulin-stimulated AC1 activity to date with reduced off-target liabilities and improved drug-like physicochemical properties making them promising lead compounds for the treatment of inflammatory pain.

INTRODUCTION

Adenylyl cyclases (ACs) are effector enzymes downstream of various G protein-coupled receptors (GPCRs) and ion channels that transduce signals via the catalysis of adenosine triphosphate (ATP) to cyclic adenosine 3',5'-monophosphate (cAMP).[1] In line with the many roles of the numerous GPCRs and ion channels, modulation of ACs leads to a variety of physiological effects dependent on the AC isoform, interaction partners, and tissue localization. Humans encode nine membrane-bound ACs that are organized into four groups based on their regulatory mechanisms to various intracellular stimuli.[2,3] Group 1 ACs include AC1, AC3, and AC8 and are characterized by their positive modulation by Ca^{2+}/Calmodulin (CaM) although AC3 is conditionally stimulated by this complex and requires the presence of additional G protein subunits.[4] Group 2 ACs include AC2, AC4, and AC7 and are conditionally activated by G protein βγ (Gβγ) subunits.[5] Group 3 ACs include AC5 and AC6 and are negatively modulated by Ca^{2+}.[6] Finally, Group 4 contains only AC9, which is the lone isoform relatively insensitive to forskolin, an allosteric agonist of ACs.

Processes such as memory acquisition, drug tolerance and dependence, and chronic pain are known to be impacted significantly by ACs.[7,8] Although ACs are expressed ubiquitously throughout the body, certain isoforms have distinct tissue expression patterns.[9] AC1 and AC8 are primarily expressed in the central nervous system (CNS) within regions such as, but not limited to, the hippocampus and the anterior cingulate cortex (ACC); regions of the brain associated with learning, memory and the development of chronic pain.[9–12] Evidence suggests AC1 is responsible for propagation of inflammatory pain stimuli.[13] *In vivo* studies indicate that injury leads to increased postsynaptic Ca^{2+} influx in the ACC, where Ca^{2+} forms a complex with CaM that, in turn, binds and subsequently activates AC1 to produce cAMP.[14,15] In chronic pain, it is suggested

that persistent Ca^{2+} influx causes hyperactivation of AC1 and downstream pain sensitization.[16] Moreover, AC1 knockout ($AC1^{-/-}$) and AC1/8 double knockout (DKO) mice exhibit nearly complete abrogation of behavioral pain response when treated with an inflammatory cocktail, complete Freund's adjuvant (CFA), and display a lack of pain sensitization in a muscle pain model.[13,17,18] However, both AC1 and AC8 are implicated to play a role in long-term memory and long-term potentiation in these brain regions.[19–21] In mouse knockout models, DKO mice displayed severe impairment to spatial memory acquisition; however, this impairment was mostly absent in the $AC1^{-/-}$ mice.[19,22–25]

Additionally, ACs propagate signals downstream from the μ-opioid receptor (MOR), a well characterized target for analgesic pharmacological therapy. MOR agonists act, in part, by negatively regulating AC1.[18] Upon agonist stimulation the MOR activates and induces dissociation of a heterotrimeric G protein complex comprised of G protein αi ($G\alpha_i$) and Gβγ subunits. The $G\alpha_i$ subunit can then translocate to a membrane bound AC, in this case AC1, and subsequently inhibit catalysis and reduce intracellular cAMP levels.[26] Additionally, chronic opioid administration leads to compensatory neuroadaptation, including upregulation of AC1 to offset the reduced cAMP signal and ultimately leading to tolerance and dependence.[18,27,28] Moreover, activation of the MOR signaling pathway has several undesired side effects, some of which are mediated by recruitment of β-arrestins and the release of Gβγ, which can lead to the development of physiological tolerance and may also contribute to opioid-induced respiratory depression, respectively.[29–31] Furthermore, MOR expression is not limited to the brain but is also expressed peripherally, leading to other common side effects such as opioid-induced constipation.[32] One potential approach under investigation to limit these side effects is the development of biased MOR agonists that favor signaling through the G protein pathway and reduce the β-arrestin pathway signal.[33] Alternatively,

our group and others have shown it is possible to target the activity of the downstream AC directly, bypassing the MOR entirely.[34–36] This strategy would allow for effective inhibition of chronic pain through AC inhibition, while avoiding negative side-effects induced by clinically used MOR agonists; thus, increasing the therapeutic index. Taken together, the promising genetic evaluation coupled with the tissue localization at the key pain center of the brain and its role in analgesic response to opioid agonists all suggest AC1 is a promising target for development of novel pharmacological modulators for the treatment of chronic pain.

Based on the aforementioned *in vivo* genetic data, a key requirement for a suitable AC1 modulator for chronic pain therapy is that it must be selective for AC1 versus AC8 to avoid the potential for memory impairment. Our group and others have since screened and tested for such modulators; the resultant known AC1 inhibitors and modulators include the adenosine-based SQ22536,[37] the adenosine-based NB001,[36] the chromone ST034307,[34] and the oxadiazole AC10065[35] (**Figure 1**). However, each molecule presents drawbacks and challenges for potential use as a pharmacotherapeutic agent. SQ22536 is proposed to bind the catalytic site of AC, and while it displays cellular potency of >10 μM (IC_{50}) versus AC1 it lacks selectivity versus other isoforms including AC5.[38] NB001 likewise has only 14-fold selectivity for AC1 versus AC8 in cell-based assays. Given that both of these compounds have adenine moieties, there is concern for selectivity versus other adenine-binding and ATP-binding proteins that could lead to off-target effects *in vivo.*[39] Our group previously published the chromone ST034307, which has a 2.3 μM IC_{50} versus Ca^{2+}/CaM-stimulated AC1 activity in cells with no inhibition of AC8.[34] This selective modulator was then shown to produce analgesic effects versus inflammatory pain *in vivo*. Despite this activity, the molecule presented significant physicochemical liabilities, namely poor aqueous solubility which hampered dosing. Furthermore, SAR was found to be intractable beyond the

published data. In the interest of finding a scaffold with tractable SAR and better drug-like characteristics, a high-throughput screen was undertaken followed by SAR elucidation of the oxadiazole series, yielding the most recent AC1 modulator AC10065.[35] This compound inhibited AC1-mediated Ca^{2+}/CaM-stimulated cAMP production in cells with an IC_{50} of 1.4 μM versus AC1 and 4.1 μM versus AC8, and displayed modest *in vivo* efficacy in a mouse CFA inflammatory pain model.[35] However, the oxadiazole series was once again limited in dosing due to the scaffold's poor aqueous solubility. In summation, these current AC1 modulators suggest that AC1 inhibition can produce anti-allodynic effects in behavioral animal studies and that isoform selectivity between AC1 and AC8 is achievable.

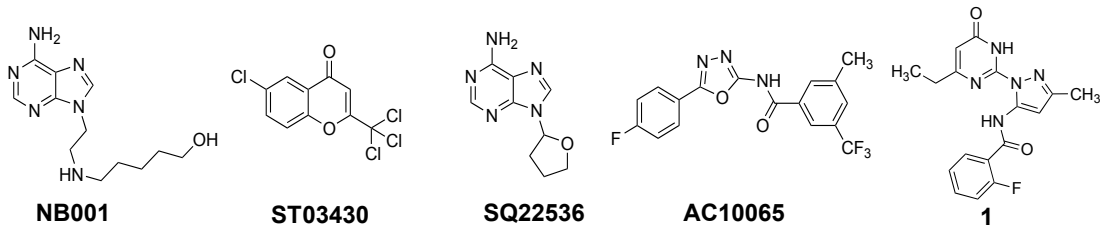

Figure 1. Representative structures of the current state of AC1 inhibitors and pyrimidinone hit **1**.

Building upon our previous work, we identified a pyrimidinone scaffold of AC1 modulators from the same high-throughput screen used to discover the oxadiazole series. These pyrimidinone AC1 modulators, represented by hit **1**, displayed similar potency as ST034307 and AC10065 while maintaining selectivity versus AC8. After resynthesizing and validating these hits, they were found to be potent and selective for inhibiting Ca^{2+}/CaM-stimulated AC1 activity over AC8, with maximal inhibition versus AC8 of 25-50% at the highest concentrations tested. Our team then designed and synthesized the following series of pyrimidinone analogs to elucidate the SAR, improve potency versus AC1, and maintain selectivity. Following activity testing a prioritized analog was chosen for *in vivo* testing in the behavioral CFA-inflammatory pain model.

Our results detailing the discovery of a sub-micromolar inhibitor of AC1-mediated Ca^{2+}/CaM cAMP production with selectivity versus AC8 and other AC isoforms are described below.

RESULTS

High-throughput screen for the discovery of inhibitors of Ca^{2+}/CaM stimulated activity of AC1

To discover additional potent and selective inhibitors of AC1 activity, our team designed and carried out a high-throughput screen of 10,240 compounds from the Life Chemical diversity library. Our primary screen sought to identify molecules that inhibit AC1 mediated Ca^{2+}/CaM-stimulated cAMP production in HEK cells stably expressing AC1 (HEK-AC1). HEK-AC1 cells were stimulated with the Ca^{2+} ionophore A23187 and the accumulation of cellular cAMP levels was quantified using a homogenous time resolved fluorescence (HTRF) assay with cAMP detection reagents as described previously.[34,35] The AC1 inhibitor ST034307[34] served as a positive control and DMSO as negative control, and the Z'-value for the screening assay was determined to be 0.6. The fluorescence values were normalized for cAMP levels of the DMSO (0% inhibition) and ST034307 (100% inhibition) controls on each plate, and hits were defined as those compounds that exhibited ≥ 90% inhibition of AC1-mediated Ca^{2+}/CaM-stimulated cAMP production at a single dose of 10 μM. A total of 480 compounds met this criterion, representing approximately 5% of the library screened. The 480 compounds were filtered for pan-assay interference compounds (PAINS)[40,41] of which 200 molecules were identified to contain PAINS-like substructures and were triaged. The remaining 280 hits were clustered into scaffolds with a Tanimoto cutoff of 70% similarity. This resulted in nine representative clusters containing, each having at least 8 compounds.

Two representative hit compounds per cluster were selected to further validate the inhibitory effects of each structural scaffold on AC1 activity and counter-screened for AC8-mediated Ca^{2+}/CaM-stimulated cAMP production. Dose-response curves were generated for each compound in HEK-AC1 cells and HEK-AC8 cells to quantify potency and AC8 selectivity. Hits were also assessed for cell viability using CellTiter-Glo to eliminate potential false-positives as a result of cell toxicity. Four clusters appeared to be false positives and were removed from further consideration. An additional cluster was excluded from further analysis because the compounds interfered with the fluorescence emission at 620 nm of the cAMP HTRF detection technology. The compounds from the remaining four scaffolds showed a dose-dependent inhibitory effect on AC1-mediated Ca^{2+}/CaM-stimulated cAMP production with IC_{50} values in the low micromolar range. Distinctively, the confirmed hit compounds of two clusters, an oxadiazole scaffold and a pyrimidinone scaffold, stood out from the rest of hits as their IC_{50} values were in the single-digit micromolar range and the compounds displayed no apparent toxic effects on the HEK-AC1 cells after 2-hour incubation. Results from optimization of the oxadiazole scaffold have since been reported leading to the development of AC10065.[35] The other single-digit micromolar potency scaffold was the pyrimidinone series represented by hit **1** (**Figure 1**) and the concentration-response curves for against AC1 and AC8 are presented in **Figure 2**.

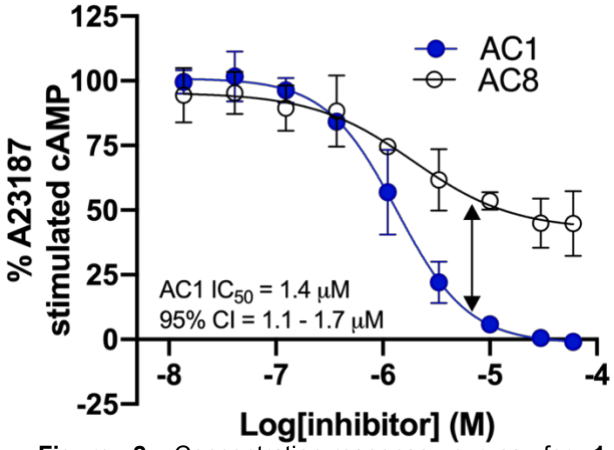

Figure 2. Concentration-response curves for **1** against AC1 and AC8 (closed blue circles) and AC8 (open black circles). Black double arrow depicts difference in efficacy at AC1 IC_{90}.

Chemistry

The general structure of the pyrimidinone hit cluster was a 3-ring aromatic scaffold comprised of a pyrimidinone, pyrazole, and an amide-coupled phenyl for which a 5-step linear synthetic sequence was designed. The pyrimidinone portion of the scaffold (**Scheme 1**) was synthesized via initial cyclocondensation of thiourea and ethyl 3-oxopentanoate to produce 6-ethyl thiouracil intermediate (**2**).[42] Intermediate **2** was selectively *S*-methylated with a slight excess of methyl iodide starting at 3 °C and was allowed to warm to room temperature producing intermediate **3**.[43] Nucleophilic substitution of **3** with hydrazine produced intermediate **4**.[44] This intermediate was then heated with 3-aminocrotonitrile and underwent a regioselective cyclization creating the pyrazolo-pyrimidinone intermediate **5.**[45] Finally, after extensive troubleshooting with numerous amide coupling protocols including benzoyl chloride and standard amide coupling, a procedure adapted from literature[46] using fluoro-*N*,*N*,*N*',*N*'-bis(tetramethylene)formamidinium hexafluorophosphate (BTFFH) to produce sterically minimal benzoyl fluoride intermediates was

able furnish low to moderate yields for the final amide products **1**, **6**, **9–32**, **36–40**. The methoxymethyl containing analog **32** was deprotected to yield the phenol **33**. Yields for analogs with electron-rich benzoic acids (e.g. **21–26**) were below the quantity necessary for biological testing, thus further optimization led to a final reaction using lithium bis(trimethylsilyl)amide (LiHMDS) pre-activation of the primary amine alongside in situ benzoyl fluoride activation of benzoic acids to provide yields sufficient for testing for these more synthetically-challenging analogs.

Several analogs required alternate methods to prepare (**Scheme 2**). Compound **7** was a product of an unintended side reaction with 2-acetoxybenzoic acid, which yielded only the acetyl substituted arylamine rather than the intended benzamide coupling product. Compound **8** was prepared via traditional HATU amide coupling as the acyl fluoride procedure did not yield the intended product. Finally, analogs **34** and **35** were found to be incompatible with either acyl fluoride coupling procedure and no desired product was obtained. In the case of **35**, according to the literature[46] carboxylic acids with α-protons were found to be incompatible with the acyl fluoride method due to competing ketene generation (despite successful synthesis of later analog **36**). In the case of **34**, the electron-donating character of the 4-dimethylamino substituent on the carboxylic was likely a contributing factor to the inability to isolate product. This led us to scout several amide coupling methods and ultimately the use of a mixed anhydride coupling method using propylphosphonic anhydride (T3P)[47] was employed to obtain **34** and **35.**

Scheme 1. Synthetic Route for Analogs 1, 6, 9 – 33, 35 – 40.[a]

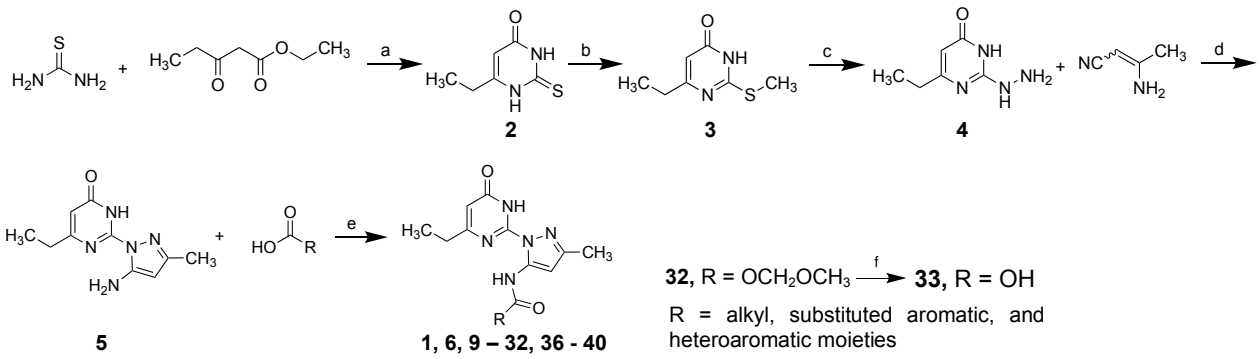

[a]Reagents and conditions: (a) KOH (1.1 eq), EtOH, 85 °C, 16 h, 61%; (b) MeI (1.2 eq), NaOH (1.1 equiv), H_2O, 3 - 23 °C 16 h, 92%; (c) hydrazine hydrate (5 equiv), K_2CO_3 (1 mol %), 2-propanol, 90 °C, 16 h, 41%; (d) 3-aminocrotonitrile (2 equiv), EtOH, 90 °C to 60 °C, 16 h, 61%; (e) A) BTFFH, DIPEA, DCM, rt to 90 °C, 16 h, 4.1−49%; OR B) 1) LiHMDS, THF, 23 °C, 30 min, 2) BTFFH, DIPEA, DCM, 23 °C, 30 m; 3) 100 °C, 16 h, 9.8−49%; (f) TFA, DCM, 0 °C, 3 h, 40%.

Scheme 2. Synthetic Route for Analogs **7**, **8**, **34**, **35**.[a]

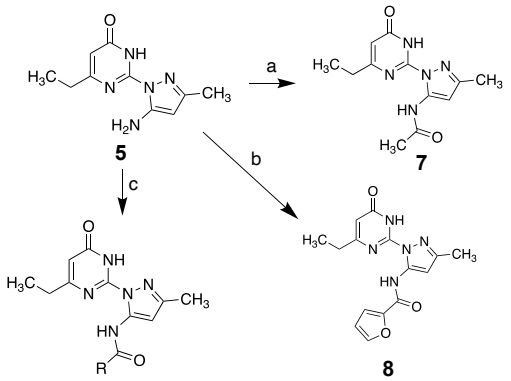

[a]Reagents and conditions: (a) 2-acetoxybenzoic acid (1.5 eq), T3P (2 eq), pyridine (3 eq), 2-MeTHF, EtOAc, 100 °C, 12 h, 34%; (b) furan-2-carboxylic acid (3 eq), DIPEA (4.2 eq), DMF, 85 °C, 18. H, 10%; (c) for **34** use 4-(dimethylamino)benzoic acid (1.5 eq) and for **35** use 2-(2-fluorophenyl)acetic acid (1.5 eq) with T3P (2 eq), base (4 eq), MeCN, HFIP, 90 °C, 16 h, 3-27%.

Structure-Activity Relationship Studies

All analogs were tested for inhibition of both AC1- and AC8-mediated Ca^{2+}/CaM-stimulated cAMP production in a cellular assay. For these activity assays, HEK293 cells had endogenous AC3 and AC6 isoforms knocked out using CRISPR-Cas9 followed by subsequent stable transfection and overexpression of AC1 or AC8 isoforms.[48] SAR was informed based on potency against AC1-mediated cAMP production. However, in terms of evaluating selectivity against AC8 a simple comparison of IC_{50} values does not adequately convey this measure. This is because in the concentration-response curves it was observed that inhibition often reaches baseline levels for AC1 at the higher molecule concentrations while AC8 is never fully inhibited by any analog (representative curves for **1** shown in **Figure 2**). This indicates that the scaffold displays a difference in maximal inhibitory efficacy between isoforms; therefore, merely evaluating the AC8 IC_{50} to assess selectivity is misleading as the IC_{50} is generated from the relative maximum and minimum cAMP signal for AC8. Case in point, analog **1** has a calculated IC_{50} value of 1.6 μM against AC8 even though it clearly is never fully inhibited. Thus, a more accurate measure of selectivity for AC1 over AC8 would be the evaluation of the percent inhibition of AC8 at the IC_{90} of AC1 activity (**Figure 2**, black arrow). Therefore, the AC8 activity will be referred to in this context. All AC1 IC_{90}s are reported in **Table S1** and concentration response curves for all molecules against AC1 and AC8 are included in the supporting information.

Initial hit compound **1** was identified in the primary screen as a potent, selective inhibitor of Ca^{+2}/CaM-stimulated AC1 activity. After re-synthesis and validation, it was found to have a cellular IC_{50} of 1.4 μM versus AC1-mediated cAMP production and 46% inhibition versus AC8-mediated cAMP production at the AC1 IC_{90}. This AC1 potency was comparable to, or an

improvement upon, the prior art for AC1 inhibitors and this scaffold was prioritized for optimization. Removal of the fluorine to yield unsubstituted phenyl derivative **6** displayed slightly reduced potency with an IC_{50} of 2.4 μM versus AC1. We then evaluated a group of analogs containing phenyl ring replacements in compounds **7**–**9**. The phenyl ring was removed leaving an acetamide in compound **7**, which showed a complete loss of activity against both ACs. Two bioisostere substitutions, a furan (**8**) and a pyridine (**9**), were assessed next. The furanyl substitution **8** was tolerated, albeit with reduced potency (AC1 IC_{50} value of 6.7 μM), whereas the pyridinyl analog **9** displayed similar activity to the phenyl (AC1 IC_{50} value of 1.2 μM) indicating the pyridine may be a suitable replacement for the phenyl without detriment to AC1 activity. However, this molecule did exhibit an increase in AC8 activity, as compared to the unsubstituted phenyl analog (**6**) but was comparable to the hit **1**. Taken together these analogs suggest optimal potency versus AC1 requires at least a 6-membered hydrophobic ring. Based on these data, we proceeded to expand the SAR exploring substitutions on the phenyl for modulation of AC1 potency and selectivity.

In the first cohort we examined the effects of fluorine, chlorine, and bromine on compound activity. No change in activity was observed moving from 2-F in **1** to 3-F in analog **10**. However, moving the fluorine to the *para*-position (**11**) provided roughly 2-fold improvement in AC1 potency an IC_{50} value of 0.79 μM while the AC8 activity was relatively unchanged. Substitution for chlorine at either the *meta*- (**12**) or *para*-position (**13**) yielded modest 2- to 3-fold improvement of potency compared to the fluorine containing counterparts with AC1 IC_{50} values of 0.47 and 0.37 μM, respectively. No improvement in selectivity versus AC8 was observed as the analogs still remained around 50% inhibition at the AC1 IC_{90} value. The 3-Br analog (**14**) displayed slightly reduced potency toward AC1 (IC_{50} value of 0.61 μM) compared to the corresponding 3-Cl,

however, this analog showed the first boost in selectivity over AC8 with only 15% inhibition of the isoform. Attempts were made to synthesize analogs with chlorine or bromine at the *ortho* position, however yields were very low for these reactions and did not provide enough material for testing.

Table 1. Potency and selectivity data for analogs against AC1 and AC8

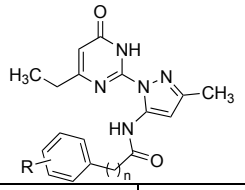

Cpd	R	n	AC1 IC_{50} (μM)[b]	AC8 Inh[c]	Cpd	R	n	AC1 IC_{50} (μM)[b]	AC8 Inh[c]
1	2-F	0	1.4 (1.1-1.7)	46%	**24**	3-$C(CH_3)_3$	0	0.88 (0.63-1.25)	25%
6	H	0	2.4 (1.9-4.6)	0%	**25**	4-$C(CH_3)_3$	0	0.97 (0.64-1.54)	35%
7	methyl[a]	0	> 30	ND	**26**	3-phenyl	0	0.25 (0.20-0.32)	37%
8	2-furan[a]	0	6.7 (4.6-19.0)	20%	**27**	4-phenyl	0	0.77 (0.53-1.12)	32%
9	2-pyridine[a]	0	1.2 (1.0-1.5)	46%	**28**	3-OCH_3	0	1.42 (0.92-2.25)	5%
10	3-F	0	1.4 (1.1-1.7)	55%	**29**	4-OCH_3	0	0.90 (0.74-1.12)	0%
11	4-F	0	0.79 (0.63-0.99)	52%	**30**	3-SCH_3	0	0.63 (0.40-0.94)	52%
12	3-Cl	0	0.47 (0.37-0.61)	48%	**31**	3-OCH_2CH_3	0	0.90 (0.73-1.1)	11%
13	4-Cl	0	0.36 (ND)	53%	**32**	4-OCH_2OCH_3	0	4.3 (3.0-6.6)	ND
14	3-Br	0	0.61 (0.46-0.82)	15%	**33**	4-OH	0	> 60	ND
15	2-CH_3	0	2.2 (1.6-2.9)	11%	**34**	4-$N(CH_3)_2$	0	2.3 (1.2-6.1)	39%
16	3-CH_3	0	0.41 (0.23-0.66)	27%	**35**	2-F	1	16.3 (ND)	ND
17	4-CH_3	0	0.67 (0.44-0.92)	27%	**36**	3-CH_3	1	9.2 (ND)	59%
18	3-CF_3	0	0.68 (0.46-0.97)	41%	**37**	2-F,3-CH_3	0	0.57 (0.35-0.96)	9%
19	2-CH_2CH_3	0	3.1 (2.6-3.7)	21%	**38**	2-F,5-CH_3	0	0.54 (0.30-0.84)	17%
20	3-CH_2CH_3	0	0.44 (0.24-0.69)	12%	**39**	3,4-di-CH_3	0	0.29 (0.20-0.43)	27%
21	4-CH_2CH_3	0	0.39 (0.10-0.65)	19%	**40**	3,5-di-CH_3	0	0.52 (0.32-0.82)	27%
22	3-$CH(CH_3)_2$	0	0.36 (0.24-0.53)	28%					
23	3-cyclopropyl	0	0.81 (0.67-0.97)	17%					

[a] Indicated groups were benzene ring replacements. [b] AC1 IC_{50}s calculated from concentration-response curves with inhibitor versus 3 μM A23187-stimulated cAMP accumulation in HEK AC1 3/6 KO cell lines (n=3+). [c] AC1 IC_{90}s were calculated from AC1 concentration-response curves and then interpolated through AC8 concentration-response curves (n=2+) and subtracted from 100%. All tabular AC1 IC_{90} data is provided in Table S1. ND = not determined by Prism software due to wide variance or not enough data points at higher concentrations.

Next, we evaluated SAR on the phenyl ring with lipophilic alkyl substituents. Similar to the halogen series, the *ortho* substituted analogs were less potent against AC1 compared to the *meta* and *para* counterparts as illustrated by a 5-fold improvement in AC1 activity when moving from the 2-methyl (**15**, IC_{50} = 2.2 μM) to the 3-methyl (**16**, IC_{50} = 0.41 μM, **Table 1** and **Figure 3A**). The improvement was more pronounced with the larger ethyl series as the 3-ethyl (**20**) was 7-fold more potent against AC1 than the 2-ethyl (**19**) derivative with IC_{50} values of 0.44 μM and 3.1 μM, respectively. Placing the methyl at the *para*-position (**17**) slightly reduced AC1 activity compared to the *meta*-methyl **16.** In contrast the 4-ethyl derivative **21** was slightly more potent than the 3-ethyl nearest neighbor with an AC1 IC_{50} value of 0.39 μM. This series of six alkyl containing analogs appeared to be generally more selective for AC1 over AC8 (11 – 28% AC8 inhibition) compared to the halogenated analogs (15 – 55%). Interestingly, swapping the 3-methyl for 3-trifluoromethyl (**18**) resulted in a slight reduction of AC1 activity but also reduced the selectivity over AC8 to 41%, which was a value closer to those observed for the halogenated analogs. Increasing the alkyl branching in this series provided mixed results. For example, moving from methyl (**16**) to ethyl (**20**) to *iso*-propyl (**22**) substitutions at the 3-position were essentially equipotent in terms of AC1 activity ranging from 0.36 – 0.44 μM while moving to the quaternary carbon with a 3-*tert*-butyl modification (**24**) reduced activity 2-fold to 0.88 μM. Moving the bulky *tert*-butyl group to the *para*-position (**25**) reduced activity further to 0.97 μM. Additionally, cyclization of the *iso*-propyl to cyclopropyl at the 3-position (**23**) resulted in more than 2-fold reduced AC1 activity at 0.88 μM compared to 0.36 μM for the *iso*-propyl derivative **22**. The tertiary and quaternary alkyl substituent also yielded slightly reduced selectivity across the board with AC8 values ranging in the 17 – 35% compared to 11 – 27% for the less branched counterparts.

Addition of phenyl substituent at the *meta*-position (**26**) yielded the most potent AC1 inhibitor synthesized with an IC_{50} value of 0.25 μM while moving the phenyl to the *para*-position (**27**) reduced potency by 3-fold. The improvement on AC1 potency for the 3-phenyl analog **26** also led to modest AC8 inhibition with 37% at the AC1 IC_{90}, which was improved from the halogenated derivatives but not as selective as the 3-ethyl analog **20**. To summarize, it appears that increasing lipophilic bulk is generally beneficial to AC1 activity, particularly at the *meta*-position while it is generally not preferred at the *para*-position. The increase of alkyl branching or addition of a phenyl functional group resulted in slightly increased AC8 inhibition compared to the methyl and ethyl analogs, although the AC8 selectivity remained less than 50% inhibition at the AC1 IC_{90} concentration for each analog. The best combination of AC1 potency with reduced AC8 inhibition appear to be the ethyl derivatives **20** and **21** with AC1 IC_{50} values of 0.44 and 0.39 μM and AC8 inhibition of 12% and 19% followed closely by 3-phenyl analog **26** with an AC1 IC_{50} value of 0.25 μM and AC8 inhibition of 37%. Dose-response curves for analog **20** are shown in **Figure 3B** and dose-response curves for all analogs are provided in supporting information.

Next, while the analogs made to this point have exhibited mid-nanomolar levels of potency in the cellular assays we observed that aqueous solubility may be a liability for the series despite the molecules possessing favorable predicted physicochemical properties from QikProp (Schrödinger, LLC; average molecular weight = 354 g/mol and QPLogPo/w = 2.55, full QikProp data set provided in a spreadsheet in supporting information). In the interest of improving aqueous solubility, we evaluated the SAR for polar substituents on the phenyl ring. The 3-OMe (**28**) and 4-OMe (**29**) displayed AC1 IC_{50}s around 1 μM versus AC1 activity accompanied with much reduced AC8 inhibition (5% and 0%, respectively). Replacement of the 3-methoxy group for the 3-thiomethyl substituent in analog **30** produced a two-fold improvement in AC1 activity but

displayed reduced selectivity versus AC8. Compounds containing bulkier polar substituents began to display reduced AC1 potency. For example, the 3-ethoxy derivative **31** possessed an AC1 IC_{50} value of 0.90 μM while the 4-methoxymethoxyl (**32**, AC1 IC_{50} = 4.3 μM) and 4-dimethylamino (**34**, 2.3 μM) substituents all showed reduced AC1 potency. The 4-hydroxy derivative **33** is noteworthy as it is the only phenyl-substituted analog in this series that showed no activity at concentrations up to 60 μM. This suggests an intolerance of a hydrogen-bond donor at the 4-position as other polar *para*-substitutions such as the 4-methoxy (**29**), 4-methoxymethoxyl (**32**), and 4-dimethylamino (**34**) still maintained AC1 IC_{50} < 5 μM**.** Nonetheless, polar functional groups led to reduced AC1 potency across the entire series.

To round out the SAR we investigated the addition of a methylene between the carbonyl of the amide and the pendent phenyl group on AC activity. Two analogs, 3-F (**35**) and 3-methyl (**36**) substituted phenyl rings, were combined with the methylene insertion. However, in each case it was observed that the methyl insertion reduced AC1 potency by about 10- to 20-fold compared to the matched molecular pair for each analog.

Finally, we synthesized analogs with combined modifications on the phenyl ring. Di-substituted compounds **37**–**40** maintain the *meta*-methyl substituent from compound **16** and combined with either a second methyl or a fluorine. Analogs **37**, **38**, and **40**, which maintained the *meta*-methyl in combination with either *ortho*-fluorine or *meta*-methyl all remained around 0.50 μM AC1 potency with low AC8 inhibition profiles. The 3,4-di-methyl analog **39** was the best of the combined modification cohort with improved AC1 potency (0.29 μM) compared to the respective mono-methyl counterparts as well as maintained the AC8 inhibition at 27%. Dose-response curves for analogs **38** and **39** shown in **Figure 3C** and **D**, all remaining dose-response curves are provided in supporting information.

To summarize, the SAR for AC1 potency and AC8 selectivity favored small, alkyl substituents over halogenated analogs for both activity metrics. Increased alkyl branching generally led to both reduced activity against AC1 and selectivity over AC8. Polar functional groups were tolerated but displayed reduced AC1 potency with the exception of the 4-hydroxy, which was the only substituted phenyl analog to display a complete loss of AC1 activity. Combined modifications produced mixed results with mid-nanomolar range AC1 potencies but slightly improved AC8 selectivity. Several analogs are within a range for AC1 activity and AC8 potency that would make them reasonable to advance toward *in vivo* efficacy assays, thus, we prioritized analogs **16**, **20**, **38** and **39** for further evaluation (dose-response curves provided in **Figure 3**).

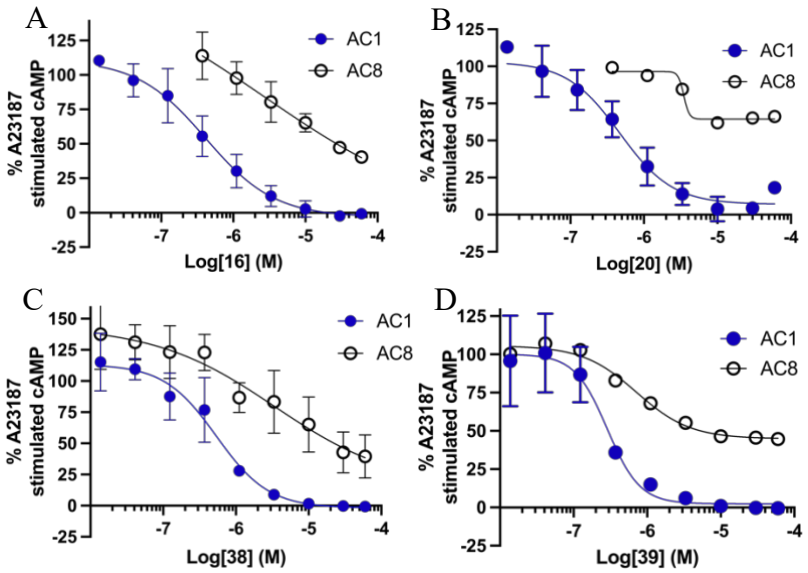

Figure 3. Overlaid AC1 (blue circles) and AC8 (open circles) dose-response curves for prioritized analogs **16** (A), **20** (B), **38** (C), **39** (D).

During the course of performing the cAMP accumulation assay in the HEK-AC1 cells we routinely assay for molecule toxicity to ensure the measured cAMP levels are descriptive of the living cellular environment. Upon initial investigation of the hit **1** there was no apparent cellular

toxicity in the HEK cells utilized for the assay. However, to ensure that the molecules did not have undesired cytotoxicity we assessed compounds **16**, **20**, **38**, and **39** in the CellTiter-Glo assay when incubated with HEK293 cells at 30 µM for 1 hour. Across the group of five analogs there was no reduction in cell viability indicating the scaffold is non-toxic to this human cell line (**Table S2**).

Analog activity in alternative AC stimulating condition and versus other AC isoforms

As selectivity is a critical parameter for AC1 inhibitors to be considered for clinical use, we examined the activity profile of the pyrimidinone scaffold for potency against other AC isoforms (**Figure 4**, **Table S3**). Screening versus representative Group I, II, and III AC isoforms showed partial inhibition of Ca^{2+}/CaM-stimulated AC8 activity, weak potentiation of Phorbol 12-myristate 13 acetate (PMA)-stimulated AC2 activity, and no apparent effect on forskolin-stimulated AC5 activity (**Figure 4)**. This data supports that the scaffold is selective for AC1 against not only the Ca^{2+}/CaM-stimulated AC8 but also against AC isoforms that are differentially activated.

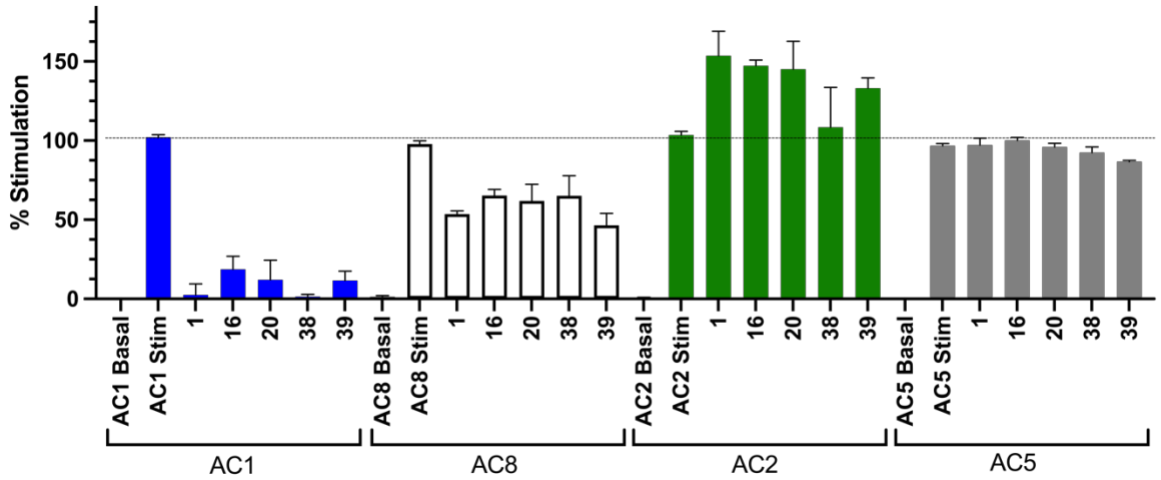

Figure 4. Inhibitory activity for five analogs against Group-1 ACs, AC1 (blue) and AC8 (white), as well as group-2 AC2 (green) and Group-3 AC5 (gray). Y-axis shown as percent stimulation of cAMP normalized to 100 % for each isoform. X-axis indicates treatment condition or analog tested. Basal indicates cAMP levels prior to stimulation. Stim indicates cAMP levels after stimulation and treated with DMSO control. All analogs tested at 10 µM (n = 3+ replicates). Error bars indicate standard error of the mean.

Activity versus common neurological off-targets

The original hit (**1**) and selected analogs (**16**, **20**, and **39**) were screened for binding against a panel of common neurological off-targets conducted by the National Institute of Mental Health Psychoactive Drug Screening Program (PDSP). In total the panel includes 44 targets including various GPCRs and ion channels. The molecules were assessed for the ability to displace radioligands from each target at a single concentration of 10 μM. In general, all molecules revealed limited significant binding with many neurological targets including the chronic pain relevant MOR, DOR, and KOR (**Table S4**). Molecule **1** was selected for secondary follow-up binding assays in dose-response to validate the primary assay binding against four targets with elevated mean % binding values: serotonin 2B (5-HT_{2B}), benzodiazepine rat brain site, muscarinic acetylcholine-2 receptor, and sigma-2 receptor. Of the four targets selected for secondary binding molecule **1** only displayed binding to 5-HT_{2B} with a K_i value of 1.3 μM while the other three did not exhibit displacement of the radioligand at concentrations up to 10 μM in the secondary validation. The same was observed for analog **16** upon secondary dose-response against 5-HT_{2B} with a K_i value of 0.9 μM. Both analogs **20** and **39** also displayed primary displacement of the radioligand from 5-HT_{2B} at 49 and 32%, respectively. While binding to 5-HT_{2B} may indicate a potential undesired off-target liability the binding assays do not assess functional efficacy at the receptor. Thus, all four analogs were further evaluated for functional efficacy against 5-HT_{2B} transfected into HEK cells in both agonist and antagonist modes. Non-transfected HEK cells served as controls. The compounds displayed no agonist activity against the 5-HT_{2B} receptor for Gq stimulation or β-arrestin recruitment in the Tango assay[49] that monitors β-arrestin translocation (**Table S5**). Likewise, no antagonist activity was observed in the Gq/Ca^{2+} assay using a calcium sensitive reporter; however, there was consistent inhibitory activity observed in the antagonist

Tango assay with IC_{50} values ranging from 0.42 – 0.60 μM. The somewhat contrasting results in the Gq/Ca^{2+} and β-arrestin antagonist assays are perplexing and may reflect a complex pharmacology requiring further study or may be due to compound interference with the Tango assay. The latter is supported by data revealing that compounds **20** and **39** that weakly bind the 5-HT_{2B} receptor (<50% displacement at 10 μM; Table S4), yet inhibit in the Tango assay with submicromolar potency.

Given that four analogs displayed relatively selective profiles from the PDSP the data was not collected in full for analog **38**, however the molecule was assessed separately for activity against the MOR, KOR, and DOR as these are relevant to the pain signaling process. The data confirms that analog **38** did not display any significant off-target modulation of the ORs at 10 μM (**Table S6**) similar to **1**, **16**, **20,** and **39**. The data as a whole suggests that this compound series is not inhibiting AC1 activity through agonism of a known $G_{i/o}$-linked GPCR.

Activity versus off-target kinases and hERG

The scaffold was further evaluated for off-target liabilities against the human Ether-á-go-go related gene (hERG) potassium channel and a select group of kinases. First, the pyrimidinone moiety bears resemblance to previously reported kinase inhibitors.[50,51] To determine the potential liability that off-target kinase inhibition may render we selected four kinases that are earmarked by pharmaceutical companies as 'sentinel representatives' of kinase families that should be assessed for pre-clinical profiling to reduce safety-related drug attrition.[52] Analogs **20**, **38**, and **39** were selected to be assessed against this small panel for inhibitory activity at a single dose of 10 μM. We found that analogs **20** and **38** did display inhibition of insulin receptor kinase (IRK) at

57% and 64% inhibition, respectively (**Table S7**). Conversely, analog **39** only exhibited 4% inhibition against IRK. For the remaining kinases, analog **20** displayed 28% inhibition versus vascular endothelial growth factor receptor-2 (VEGFR2) but did not exhibit any inhibition toward leukocyte C-terminal Src kinase (LCK) or Rho-associated coiled-coil containing kinase (ROCK1). Analogs **38** and **39** did not inhibit any of the remaining three kinases tested. Therefore, while analogs **20** and **38** displayed appreciable activity against IRK the inhibition does not appear to be intrinsic to the scaffold as **39** was inactive against these targets. Nevertheless, it would be prudent to continue to monitor analog effects on kinases and expand the panel for future studies.

Finally, both analogs were also evaluated for ability to bind to the hERG potassium channel to assess for potential cardiac liability. Analog **20** displayed 0% inhibition of [^{3}H]-astemizole binding at a dose of 10 μM while **38** and **39** exhibited 6% and 11% inhibition at the same dose (**Table S6**). No molecule was determined to be a significant hERG binder.

In silico and in vitro physicochemical and pharmacokinetic properties of prioritized analogs

This class of molecules did display reduced solubility in aqueous media, thus, we first assessed thermodynamic solubility experimentally for the four prioritized analogs using a method previously described.[53,54] This analysis showed **38** was the most soluble at 33.6 μM in PBS at pH 7.4 and 25 °C, which is approximately 60-fold higher than the cellular IC_{50} for inhibition of Ca2+/Calmodulin-stimulated AC1 activity. This was followed by **16** (19.5 μM), **20** (10.8 μM) and **39** (7.6 μM) in decreasing order of solubility (Table 2).

Next, as a means to select a candidate for evaluation in an *in vivo* model for inflammatory pain, cheminformatics analysis of physicochemical and pharmacokinetic properties was carried out using QikProp (Schrödinger, LLC). Molecules were loaded into Maestro and prepared for computational analysis. Using the OPLS3e force field the protonation states at pH 7.4 were determined and energy minimization was performed. Since the presumed site of action for our compounds is in the CNS we have given consideration to molecular properties that could affect blood-brain barrier (BBB) permeability. Several analyses have been published on physicochemical properties that drive BBB permeability and in general the consensus is that molecules with molecular weight < 400 g/mol and LogP ranging from 2 – 5 have increased probability for CNS activity.[55–58] The molecular weights of the four prioritized analogs range from 337 g/mol to 355 g/mol and QPLogPo/w ranged from 2.32 – 2.88 (specific values for selected analogs provided in **Table 2**). Conversely, the Polar Surface Area (PSA) for the analogs is maintained around 100 Å^2. This may be detrimental to CNS activity as PSA < 90 Å^2 is desired for small molecule CNS activity[56,59] with an ideal range between 40 – 80 Å^2.[60,61] Related is the hydrogen-bond donors (HBD) and acceptors (HBA) counts for the prioritized analogs. The number of HBD (2 for each molecule) and HBA (7 for each molecule) are at the upper preferred limit desired for CNS active molecules.[60]

These properties are combined within QikProp to provide two predictive metrics for CNS permeability that have been benchmarked with experimental data[62]: 1) the CNS score and 2) QPPMDCK. The CNS score is a multiparameter-based metric on a scale of -2 (inactive) to +2 (active). Based on these calculations, analogs **16**, **20**, and **39** all are predicted to be CNS inactive with values of -2 for each while **38** has a predicted value of 0, indicating at least partial CNS activity. Alternatively, Madin-Darby Canine Kidney (MDCK) cells have been shown to be a viable

surrogate to assess for BBB permeability.[55,63] This is captured in the QPPMDCK apparent permeability (P_{app}) metric where a predicted P_{app} > 500 nm/sec is desired for CNS activity. Analogs **16**, **20** and **39** all had QPPMDCK P_{app} values around 140 nm/sec, which would support the reduced CNS score, while **38** was predicted to have a value of 632 nm/sec (Table 2) indicating it was the most likely of the cohort to reach the desired site of action. A full data set of QikProp metrics for all analogs is provided as a spreadsheet in the supporting information.

Table 2. Predicted and experimentally determined physicochemical and pharmacokinetic metrics

Cpd	MW (g/mol)	QPLogPo/w[a]	PSA (Å^2)	CNS[b]	QPPMDCK (nm/sec)[c]	Solubility (μM)[d]	P_{app} (nm/sec)[e]
Desired Ranges	< 400	2 - 5	< 90	0 – 2	> 500	10x AC1 IC_{50}	-
16	337	2.32	100.5	-2	141	19.5	nt
20	351	2.65	100.5	-2	141	10.8	nt
38	355	2.88	101.4	0	632	33.6	22.1
39	351	2.57	100.5	-2	140	7.6	nt

[a] QikProp metric for predicted octanol/water partition coefficient. [b] QikProp multiparameter-based predictive metric for molecules CNS activity. Ranges from -2 (inactive) to +2 (active). [C] QikProp predictive metric for apparent MDCK cell permeability. [d] Thermodynamic solubility in PBS at pH 7.4 and 25 °C determined according to previously described protocol.[53,54] [e] Experimental apparent MDCK permeability.

Based on the measured solubility and computational predictions for CNS activity we selected analog **38** to be assessed for experimental MDCK permeability. The molecule displayed a P_{app} from apical to basolateral of 22.1 nm/sec, well below the predicted value for QPPMDCK. Regardless, even though **38** displays reduced MDCK permeability it is still comparable to, or better than, other known CNS active drugs.[55,64–66]

As **38** emerged as our lead molecule from this series we performed further cheminformatic absorption, metabolism, distribution and excretion (ADME) analysis using pkCSM[67] to identify potential ADME liabilities. This *in silico* analysis uses graph-based signatures of molecules to compare against training sets of molecules with known ADME properties. This analysis flagged

the **38** as a potential inhibitor cytochrome P450s (CYP) 1A2 and 3A4 and substrate of CYP3A4 and CYP2D6. Metabolism and inhibition of CYPs can adversely impact the metabolic profiles of the lead molecule and other drugs taken in combination.[68] Thus, the effect of small molecules on CYPs should be assessed to de-risk the scaffold for lead optimization. To this end, we evaluated **38** for inhibition at five CYPs that contribute to metabolism of over 50% of marketed drugs.[68,69] The molecule was dosed at a single concentration of 10 μM and evaluated for percent inhibition. In contrast to the pkCSM predictions it was found that **38** had no significant inhibition of any of the five CYPs tested in this panel (**Table 3**).

Table 3. In vitro CYP and metabolic profile for analog **38**

% CYP Inhibition at 10 μM[a]					HLM Stability (% remaining) [b]					
1A2	**2C19**	**2C9**	**2D6**	**3A4**	**15 min**	**30 min**	**45 min**	**60 min**	**$t_{1/2}$[c]**	**CL_{int}[d]**
8.7	1.8	-0.2	0.3	-0.9	88.3	67.4	57.5	44.5	51.2	136.7

[a] % inhibition is calculated by subtracting from untreated controls. [b]HLM = human liver microsome. Tested at 37 °C in 0.1 mg/mL HLMs. % remaining is percentage of compound remaining in sample at each time point and is average of 2 replicates. [c] Half-life of molecule in minutes. [d] Intrinsic clearance of molecule from HLMs in μL/min/mg.

Alternatively, we sought to assess the potential for metabolic modification of the molecule by quantifying stability in human liver microsomes (HLM). It was found that compound **38** is metabolized in the HLM assay with 88% of molecule remaining at the 15-minute time-point followed by steady decline to 45% remaining at the 60-minute timepoint. This analysis yielded a half-life ($t_{1/2}$) of approximately 51 minutes and intrinsic clearance (Cl_{int}) of 136.7 μL/min/mg (**Table 3**). On the basis of the physicochemical, *in vitro* pharmacokinetic properties and relatively benign safety profile against off-targets for analog **38** we chose to move this molecule forward for testing in the mechanical allodynia mouse model.

*In vivo efficacy of compound **38** in a mouse model for inflammatory pain*

To assess whether **38** could reduce pain sensitization we evaluated the analog in a mouse model for inflammatory pain with CFA as previously published.[34,35] Compound **38** was injected intraperitoneally (*i.p.*) at a dose of 5.6 mg/kg and was compared to 5.6 mg/kg morphine (positive control) and vehicle (negative control). Mechanical allodynia was quantified by von Frey filament testing recorded pre-CFA injection (no allodynia), 24-hr post-CFA injection (0 min, allodynia), and over a period of 2 hours post-treatment with **38** or morphine. Compound **38** displayed modest, yet statistically significant, anti-allodynic effects in this inflammatory pain model at 1-hour post-treatment compared to the 0 min (allodynic) time point (**Figure 5**). Morphine produced a more pronounced anti-allodynic effect throughout the time course.

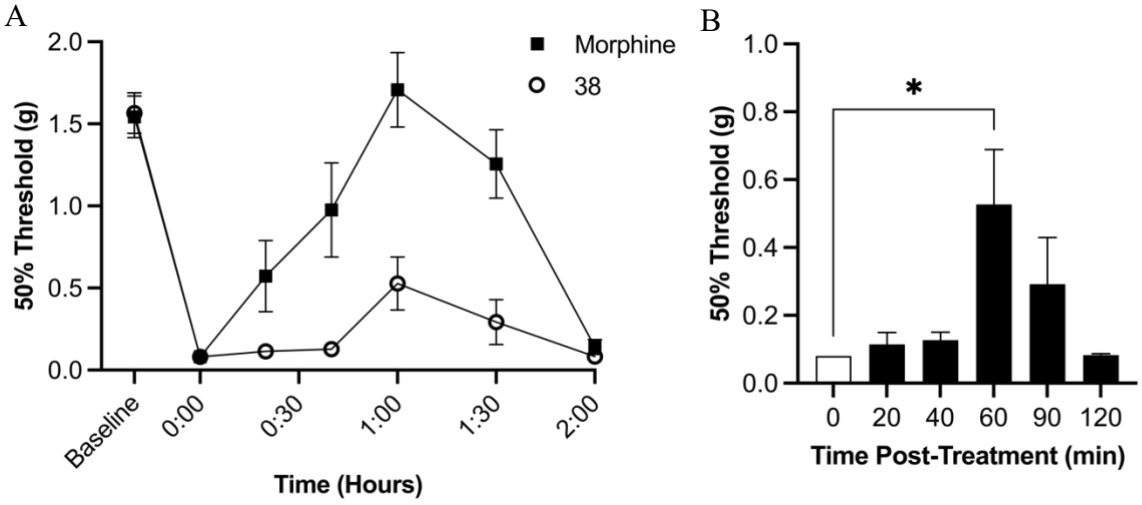

Figure 5. Anti-allodynic Effect of Compound **38** in the CFA Inflammatory Pain Model. Mechanical thresholds were determined using von Frey filaments. Mice were baselined then injected with 10uL of 50% CFA emulsion into the plantar region of the paw. 24 hours later mice were baselined then injected with 5.6 mg/kg morphine or 5.6 mg/kg compound **38**. Time-course taken over 2-hour period comparing **38** to morphine (A) and time-course with statistical analysis for **38** (B). Data represents the mean ± SEM of the 50% mechanical threshold (n = 6). Statistical analysis performed using nonparametric One-Way ANOVA (Friedman test), Dunn's post-hoc correction. *$p < 0.05$ versus 0 min time point.

DISCUSSION

Following our previous reports of selective AC1 inhibitors for chronic pain, we sought to discover a scaffold with improved drug-like characteristics and potency while maintaining selectivity versus AC8. The same high-throughput screen that identified the prior oxadiazole series[35] also yielded the pyrazolyl-pyrimidinone scaffold as potent AC1 inhibitors with selectivity against AC8 and having higher predicted aqueous solubility. The optimization was multifaceted as we sought to improve AC1 potency while maintaining/improving selectivity over AC8. However, during the design we were also cognizant of modifications that may improve solubility and/or BBB permeability. After SAR optimization of the benzamide moiety, we were able to improve potency by 2 – 4-fold across the series of analogs versus Ca^{2+}/CaM-stimulated AC1 activity while maintaining/improving selectivity versus AC8. The SAR revealed a 6-membered aromatic group was preferred on the amide as both the phenyl and 2-pyridine functional groups were comparable with low-micromolar potency against AC1. We moved forward with phenyl modifications for two reasons: 1) a greater availability of substituted reagents to better explore SAR and 2) we wanted to limit the number of heteroatoms in an attempt to improve BBB permeability. Hydrophobic substituents were preferred on the phenyl ring, particularly at the *meta*- or *para*-positions. Furthermore, the potent activity of analogs **26** (3-phenyl) and **27** (4-phenyl) implies a larger capacity or perhaps flexibility of the putative molecule binding site to accommodate flat hydrophobic substitutions. While the increased lipophilicity is generally helpful to improve BBB permeability it is typically is detrimental to solubility.[55,70] A few analogs that

incorporated polar functional groups such as methoxy, hydroxy, and dimethyl amino all resulted in reduced potency against AC1 activity compared to the top leads.

In terms of potency against Ca^{2+}/CaM-stimulated AC8 activity, the halogenated series was generally least selective at around 50% AC8 inhibition at the AC1 IC_{90} with the exception of the 3-Br derivative at 15% AC8 inhibition. When the substitution was switched to lipophilic alkyl functionalities there was an observed drop in AC8 inhibition at the AC1 IC_{90} for the analogs tested. For example, among analogs **15** – **27** containing hydrophobic modifications the AC8 inhibition ranged from 11 – 41%. The 3-ethyl (**20**) and 4-ethyl (**21**) derivatives were among the most selective with AC1 IC_{50} values of 0.44 μM and 0.39 μM, respectively, paired with sub-20% AC8 inhibition. Interestingly, the branched derivatives we slightly less selective than the linear alkyl counterparts.

Given that the scaffold has three aromatic rings and contains several heteroatoms that could partake in both intramolecular and intermolecular hydrogen-bonds we posited that perhaps the low solubility of the scaffold may be a function of planarity and high-crystal packing energy.[71,72] It has previously been observed that introducing contiguous rotatable bonds may reduce crystal packing and improve solubility of molecules in aqueous media.[71] Thus, analogs **35** and **36** were designed to insert a methylene between the amide carbonyl and the pendent phenyl to explore both AC1 potency and solubility. Unfortunately, the modification was detrimental to AC potency as each analog was at least 10-fold less potent compared to their nearest neighbor analogs without the extra methylene. However, qualitatively these analogs were more soluble in aqueous media compared to the matched molecular pairs, although exact measurements were not obtained because the molecules were inferior in AC1 activity. Nonetheless, for future analog design the strategy of reducing planarity of the scaffold may prove useful. Finally, when combinations of substitutions were made there was not an improvement in activity versus AC1 that was desired. Regardless, the

combined modifications in **38** did project to yield a CNS active analog according to QikProp projections. Thus, this molecule, along with three analogs in **16**, **20**, and **39** that exhibited better potency with inferior projected BBB permeability were prioritized for further evaluation in downstream assays.

In addition to AC1 and AC8, the original hit and four prioritized analogs were also tested against two other AC sub-families represented by AC2 and AC5. AC2 is a member of the group II subfamily and is conditionally activated by Gβγ subunits. AC5 is a group III sub-family enzyme and is inhibited by Ca^{2+}. It was found that when AC2 is activated by PMA that the scaffold generally potentiates AC2 activity by up to 50%, although analog **38** displayed the relatively little potentiation. This phenomenon has been previously observed for other AC1 inhibitors reported by our group[34,35] and at this point it is difficult to posit what this may mean physiologically, if anything, as there is very little understood about AC2 activity *in vivo.* AC2 is expressed in the brain, lung, skeletal muscle and heart yet there is very little understood about its physiological function and a lack of animal knockout models and selective inhibitors has kept the function elusive.[3,34] As for AC5 activity the scaffold appeared to have no modulatory effects against this enzyme that differed from the DMSO-treated controls. Therefore, the pyrimidinone scaffold appears to be selective for targeting AC1 over other isoforms.

Little is known about the scaffold at this point from an off-target perspective. The pyrazole-pyrimidine substructure has been recently reported in only one other manuscript to possess anti-leishmania properties via promoting microtubule polymerization.[73] Moreover, three analogs tested for activity against four human kinases relevant to off-target toxicity displayed moderate-to-no inhibition at a single dose of 10 μM. This would suggest that kinase inhibition may not preclude this scaffold from advancement, however, the kinases tested are not exhaustive and additional

experiments are necessary to understand the potential impact the molecules may have on the human kinome. Additionally, even though AC8 maintains significant residual activity at higher concentrations of inhibitor we still do not know if this will be sufficient to alleviate potential learning deficits similar to those observed in the AC1 and AC8 double knockout mice. Further analysis in learning and behavior assays are required to fully investigate any potential impact, or lack thereof, on learning and memory.

With the combined data showing the analog **38** displayed mid-nanomolar AC1 potency with sub-20% AC8 inhibition, little modulation at other AC isoforms, and had the best overall predicted and measured physicochemical and MDCK permeability metrics it was prioritized for testing in an *in vivo* CFA mouse model for inflammatory pain. The analog did display modest, yet significant, anti-allodynic properties in this model at the 1-hour timepoint. The results are promising for the scaffold as we believe there are still alterations to be made for improvement of the physicochemical and pharmacokinetic properties of the molecules. For example, mice were dosed *i.p.* which may reduce the amount of molecule that enters circulation at the site of action. Solubility improvements should provide a means to increase testable doses. Exploration of SAR at other parts of the scaffold may provide openings for improving BBB permeability. The investigation of this scaffold is only at the beginning stages with much yet to learn about the SAR and potentially how the molecules interact with the target intracellularly that could provide further ideas for analog design. Regardless, the pyrazolo-pyrimidine scaffold represents a previously unreported class of AC1 inhibitors that may have potential for treatment or aid in validation of AC1 inhibition as a viable therapeutic strategy for inflammatory pain and to provide alternatives to opioid analgesics.

CONCLUSION

A cell-based high-throughput screen identified the pyrazolo-pyrimidine scaffold with inhibitory activity against Ca^{2+}/CaM-stimulated AC1 cAMP production. A ligand-based SAR optimization campaign, with 36 novel analogs, explored modifications to the benzamide portion of the scaffold to improve AC1 inhibitory activity and improve selectivity over the closely related AC8. It was observed that hydrophobic substitutions on the phenyl ring at both the *meta*- and *para*-positions provided IC_{50} values as low as 0.25 μM with reduced activity against AC8. Prioritized analogs based on potency, selectivity, solubility and predicted BBB permeability were further evaluated at additional AC isoforms. The molecules were observed to potentiate AC2 activity but did not display any modulatory effect against AC5. Additionally, the prioritized analogs were largely inactive at all opioid receptors and against selected kinases. Finally, when evaluated in a murine CFA model for inflammatory pain analog **38** displayed modest anti-allodynic properties with a significant effect at the 1-hour post-treatment time point, demonstrating the potential of the scaffold for relieving pain. Further studies will focus on improvement of physicochemical and pharmacokinetic properties while maintaining AC1 potency and selectivity to enhance *in vivo* efficacy.

EXPERIMENTAL SECTION

Chemistry

General Methods. Purity of all final compounds was ascertained via HPLC on an Agilent 1200 series chromatograph >95%. Chromatographic methods utilized include a ThermoScientific Hypersil GOLD C-18 4.5 X 250 mm, 3 μm column, UV detection at a wavelength of 254 nm, flow-rate set to 1.0 mL/min, and with an acetonitrile: water gradient from 5% to 95% acetonitrile over 12 minutes with a 3 min hold time at 95%. Both acetonitrile and water contained 0.1% v/v formic acid. Mass spectrometry was obtained on an Advion CMS-L Compact Mass Spectrometer with an APCI or ESI source on normal or low fragmentation settings. ^{1}H and ^{13}C NMR spectra were recorded on either a Bruker DRX500 spectrometer or a Bruker AVIII in $CDCl_3$, DMSO-d_6, or Methanol-d_4 with internal standard of TMS at 0.05% v/v. Chemical shifts (δ) reported below are as parts per million (ppm) and the coupling constants are reported as follows: s=singlet, d=doublet, t=triplet, q=quartet, p=pentet, h=hextet, hept=heptet, dd=doublet of doublets, ddd=doublet of doublet of doublets, m=multiplet. Protocols for each compound are detailed below. Compounds were prepared according to scheme 1 and protocol is detailed below for compound **1**. All other compound synthesis and characterization data is provided in the supporting information.

6-Ethyl-2-thioxo-2,3-dihydropyrimidin-4(1H)-one (**2**). To a 250 mL round bottom flask equipped with stirbar, thiourea (5.99g, 78.7 mmol, 1 eq.) and potassium hydroxide (5.10 g, 90.9 mmol, 1.2 eq.) were added. The powders are then suspended with 60 mL of 200 proof ethanol and the mixture is heated while stirring to 75 °C. To this stirring mixture, ethyl 3-oxopentanoate (12.5 mL, 87.6 mmol, 1.11 eq.) is added in one portion. The flask was then sealed with a glass stopper and the solution is heated at 85°C overnight. White solid began crashing out of solution quickly, with the solution appearing orange/pink. After 16 hours, the suspension is removed from heat and allowed to slowly return to room temperature. The suspension was concentrated on *in vcauo* to remove

about half of the volume of ethanol (~30 mL ethanol remaining). To this suspension, deionized water was added slowly while stirring until the mixture turns completely clear. The solution was then slowly neutralized while stirring by adding concentrated HCl (12 N in water) and diluted NaOH (1.0 N in water) to pH 7.0. As the solution approaches neutral pH, white solid should begin crashing out of solution. Once the mixture was neutralized, the suspension was filtered and washed with water. The white powder was then allowed to dry on filter paper under suction before being transferred to a vial and placed on hi-vac. The resultant powder **2** was collected and taken forward without further purification (7.46 g, 47.8 mmol, 61% yield). ^{1}H NMR (500 MHz, Methanol-d_4) δ 5.70 (s, 1H), 2.43 (q, J = 7.5 Hz, 2H), 1.21 (t, J = 7.5 Hz, 3H).

*6-Ethyl-2-(methylthio)pyrimidin-4(1H)-one (**3**)*. Intermediate **2** (7.46 g, 47.8 mmol, 1 eq.) was added to a 250 mL round bottom flask equipped with stirbar. In a separate container, sodium hydroxide (2.10 g, 52.6 mmol, 1.1 eq.) was added and dissolved via sonication in 30 mL of water. This sodium hydroxide solution was then added slowly while stirring to the round bottom flask with **2**. The combined solutions were allowed to stir for 30 minutes at room temperature. After 30 minutes the solution was placed in an ice water bath (0°C) for 5 minutes (note: some solid may fall out of solution). To this stirring mixture in the ice bath was added iodomethane (3.57 mL, 57.3 mmol, 1.2 eq.). The mixture was stirred rapidly to ensure distribution of iodomethane and allowed to stir overnight inside the ice water bath as it slowly warmed to room temperature. After 16 hours the suspension was immediately filtered, washed with ice water and allowed to dry for 15 minutes on filter paper before transfer to hi-vac, yielding a white powder **3** was taken forward without further purification (7.48 g, 44.0 mmol, 92%). ^{1}H NMR (500 MHz, DMSO-d_6) δ 12.50 (s, 1H), 5.90 (s, 1H), 2.44 (s, 3H), 2.39 (q, J = 7.4 Hz, 2H), 1.09 (t, J = 7.5 Hz, 3H).

6-Ethyl-2-hydrazineylidene-2,3-dihydropyrimidin-4(1H)-one (**4**). To a 250 mL round bottom flask equipped with stirbar **3** (7.48 g, 44.0 mmol, 1 eq.), potassium carbonate (61.2 mg, 443 μmol, 1 mol %), and 30 mL of 2-propanol were added. To this stirring mixture, hydrazine hydrate (10.6 mL, 219 mmol, 5 eq., 64% hydrazine) was added in one portion. The vessel is tightly sealed with a glass stopper and heated to 80°C for 5 hours and then lowered to 60°C for 18 hours. The reaction was cooled briefly on ice and the precipitate was filtered and washed with 1 mL volumes of diethyl ether (3 times) and methanol (3 times). The resultant off-white powder was then dried on hi-vac to yield **4** without further purification (2.78 g, 18.0 mmol, 41%).^{1}H NMR (500 MHz, DMSO-d_6) δ 8.45 (s, 1H), 5.36 (s, 1H), 4.51 (s, 2H), 2.27 (q, J = 7.5 Hz, 2H), 1.08 (t, J = 7.5 Hz, 3H).

2-(5-Amino-3-methyl-1H-pyrazol-1-yl)-6-ethylpyrimidin-4(1H)-one (**5**). Intermediate **4** (2.78 g, 18.0 mmol, 1 eq.) and 3-aminocrotonitrile (2.96 g, 36.1 mmol, 2 eq.) were added to a 250 mL round bottom flask equipped with stirbar and then suspended in 30 mL of 200 proof ethanol. The vessel is sealed with a rubber stopper and vented with a 20G needle. The mixture is heated at 90°C for 4 hours then 60°C for 16 hours. The reaction was allowed to return to room temperature while stirring then chilled to 3 °C inside a refrigerator. A precipitate was then filtered and washed in sequential order with portions of hexanes (3 x 10 mL), ethanol (3 x 10 mL), methanol (3 x 10 mL), and DCM (3 x 10 mL). The resultant powder was then allowed to dry on filter before transfer to hi-vac to yield **5** no further purification (2.49 g, 11.1 mmol, 61%).^{1}H NMR (500 MHz, DMSO-d_6) δ 11.47 (s, 1H), 6.90 (s, 2H), 5.98 (s, 1H), 5.27 (s, 1H), 2.52 (q, J = 7.6 Hz, 2H), 2.09 (s, 3H), 1.16 (t, J = 7.5 Hz, 3H). APCI-MS: m/z 220.1 $[M+H]^+$.

General Procedure A for Amide Coupling

N-(1-(6-ethyl-4-oxo-1,4-dihydropyrimidin-2-yl)-3-methyl-1H-pyrazol-5-yl)-2-fluorobenzamide (**1**). Acyl fluoride amide coupling is adapted from a previously reported procedure.[46] To an oven-dried microwave vial equipped with stirbar and intermediate **5** (0.23 mmol, 1 eq.) was added. The vial was sealed tightly and evacuated under vacuum then recharged under argon atmosphere three times. To an second oven-dried microwave vial was added 2-fluorobenzoic acid (0.083 g, 0.59 mmol, 1.3 eq.) and fluoro-*N*,*N*,*N*′,*N*′-bis(tetramethylene)formamidinium hexafluorophosphate (BTFFH) (0.22 g, 0.68 mmol, 1.5 eq.). The vial was then sealed and evacuated with argon three times followed by addition of dry dichloromethane (DCM) (880 μL) and *N*,*N*-diisopropylethylamine (DIPEA) (100 μL, 0.57 mmol, 2.5 eq.). The mixture was allowed to stir for 30 minutes under argon to prepare the acyl fluoride. After 30 minutes the crude acyl fluoride solution was withdrawn from the second vial and injected dropwise into the vial containing intermediate **5** while stirring. The vial was then heated for 16 hours in a sandbath at 100 °C.

The reaction was then quenched with 1 mL deionized water, agitated vigorously, and then allowed to stir at room temperature for 15 minutes. The vial's contents were then transferred to a separatory flask and diluted with 10 mL DCM and 10 mL 1% aqueous HCl. The organic layer was separated and the aqueous layer was extracted with a second portion of DCM. The combined organic layers were then washed sequentially with equal volumes of 1% aqueous HCl, saturated sodium bicarbonate solution, and brine. The resultant organic layer was dried with $MgSO_4$, filtered and concentrated *in vacuo*. The mixture was concentrated then suspended in 1-2 mL of ethyl acetate to provide a suspension. The suspension was filtered and washed with ethyl acetate then dried to yield **1** as a white powder (0.059 g, 0.17 mmol, 38%) as a white solid. ^{1}H NMR (800 MHz, $CDCl_3$) δ 12.36 (s, 1H), 10.33 (s, 1H), 8.15 (t, J = 7.8, 3.9 Hz, 1H), 7.58 (q, J = 7.1 Hz, 1H), 7.34 (t, J = 7.6 Hz, 1H), 7.21 (dd, 1H), 6.97 (s, 1H), 6.09 (s, 1H), 2.63 (q, J = 7.6 Hz, 2H), 2.31 (s, 3H),

1.24 (t, J = 7.6 Hz, 3H). ^{13}C NMR (201 MHz, $CDCl_3$) δ 169.0, 161.2, 160.4 (d, ^{1}J = 250.2 Hz), 159.8, 153.7, 148.3, 140.4, 134.5 (d, ^{3}J = 9.1 Hz), 132.4, 125.1 (d, ^{4}J = 3.2 Hz), 120.6 (d, ^{3}J = 11.6 Hz), 116.2 (d, ^{2}J = 23.8 Hz), 107.6, 100.2, 30.1, 14.2, 12.2. APCI-MS(+): m/z 342.2 $[M+H]^+$. APCI-MS(-): m/z 340.0 $[M-H]^-$. HPLC retention time: 12.691 min. HPLC purity 99.50%.

General Procedure B for Amide Coupling (shown for 14).

3-Bromo-N-(1-(4-ethyl-6-oxo-1,6-dihydropyrimidin-2-yl)-3-methyl-1H-pyrazol-5-yl)benzamide (**14**). To an oven-dried microwave vial was added intermediate **5** (0.050 g, 0.23 mmol, 1 eq.) followed by evacuation under vacuum and flushing with argon three times. To this vial was added LiHMDS 1.0 M in THF (1.03 mL, 1.03 mmol, 4.5 eq.) was then added dropwise. The mixture was allowed to stir at room temperature for 30 minutes.

The acyl fluoride generation proceeds as described in General Procedure A in a separate microwave vial using 3-bromobenzoic acid (0.060 g, 0.30 mmol), BTFFH (0.11 g, 0.34 mmol), DIPEA (100 µL, 0.57 mmol), and DCM (0.5 mL). The activated amino-pyrazole solution from the first vial is then added dropwise to the crude acyl fluoride solution in the second vial and stirred at 80 °C for 18 hours. The reaction proceeded to be worked up the same as described in General Procedure A to provide **14** as a white solid (0.026 g, 0.064 mmol, 28%). ^{1}H NMR (800 MHz, $CDCl_3$) δ 12.43 (s, 1H), 10.31 (s, 1H), 8.07 (s, 1H), 7.96 (d, J = 8.0 Hz, 1H), 7.74 (d, J = 7.9 Hz, 1H), 7.42 (t, J = 7.9 Hz, 1H), 6.87 (s, 1H), 6.11 (s, 1H), 2.71 (q, J = 7.5 Hz, 2H), 2.32 (s, 3H), 1.30 (t, J = 7.6 Hz, 3H). ^{13}C NMR (201 MHz, $CDCl_3$) δ 168.0, 161.9, 160.9, 154.1, 148.7, 140.8, 135.7, 135.1, 130.6, 129.8, 126.5, 123.0, 107.7, 99.2, 30.8, 14.2, 12.3. APCI-MS(+): m/z 401.9, 403.9

$[M+H]^+$. APCI-MS(-): m/z 399.8, 401.8 [M-H]. HPLC retention time: 13.539 min. HPLC purity 95.3%.

N-(1-(6-Ethyl-4-oxo-1,4-dihydropyrimidin-2-yl)-3-methyl-1H-pyrazol-5-yl)benzamide (**6**). Prepared using general procedure A with benzoic acid (0.036 g, 0.30 mmol), BTFFH (0.11 g, 0.34 mmol), DCM (440 μL), DIPEA (180 μL, 1.0 mmol), and **5** (0.050 g, 0.23 mmol) to produce **6** (0.017 mg, 0.052 mmol, 23%) as a white solid. ^{1}H NMR (500 MHz, $CDCl_3$) δ 12.38 (s, 1H), 10.33 (s, 1H), 7.98 (d, J = 7.1 Hz, 2H), 7.64 – 7.59 (m, 1H), 7.53 (t, J = 7.3 Hz, 2H), 6.88 (s, 1H), 6.10 (s, 1H), 2.65 (q, J = 7.5 Hz, 2H), 2.31 (s, 3H), 1.29 (t, J = 7.5 Hz, 3H). ^{13}C NMR (126 MHz, CDCl3) δ 167.9, 163.4, 160.8, 154.0, 148.6, 141.0, 133.1, 132.6, 128.8, 127.2, 107.6, 98.9, 30.5, 14.1, 12.2. APCI-MS(+): m/z 324.1 $[M+H]^+$. APCI-MS(-): m/z 322.0 $[M-H]^-$. HPLC retention time: 12.422 min. HPLC purity 98.6%.

N-(1-(6-Ethyl-4-oxo-1,4-dihydropyrimidin-2-yl)-3-methyl-1H-pyrazol-5-yl)acetamide (**7**). Intermediate **5** (0.025 g, 0.11 mmol, 1 eq) was suspended in 2-MeTHF (500 μL) inside a microwave vial. Acetylsalicylic acid (0.031 g, 0.17 mmol, 1.5 eq) and pyridine (30 μL, 0.33 mmol, 3 eq) were added to the stirring mixture. Finally, propylphosphonic anhydride (T3P) (0.15 g 50% w/w in EtOAc, 0.23 mmol, 2 eq) was added to the mixture which was then immediately sealed. The vial was then heated to 100°C in a Biotage Initiator microwave for 12 hours. After cooling, the mixture was diluted with deionized water and agitated vigorously. The aqueous layer was then extracted with an equal volume of DCM. The organic layer was then collected, dried with $MgSO_4$, and concentrated *in vacuo*. It was then further purified via normal phase flash chromatography (2-6% v/v MeOH in DCM). Fractions containing product were concentrated and dried on hi-vac yielding **7** (0.010 g, 0.039 mmol, 34%) as an off-white solid. ^{1}H NMR (800 MHz, CDCl3) δ 11.53 (s, 1H), 10.25 (s, 1H), 6.72 (s, 1H), 6.07 (s, 1H), 2.61 (q, J = 7.6 Hz, 2H), 2.27 (s, 3H), 2.24 (s,

3H), 1.30 (t, J = 7.6 Hz, 3H). ^{13}C NMR (201 MHz, CDCl3) δ 167.8, 166.3, 160.9, 154.0, 148.6, 140.7, 107.8, 98.9, 30.3, 24.3, 14.2, 11.9. APCI-MS(+): m/z 262.0 $[M+H]^+$. APCI-MS(-): m/z 259.9 $[M-H]^-$. HPLC retention time: 10.065 min. HPLC purity 98.9%.

N-(1-(6-Ethyl-4-oxo-1,4-dihydropyrimidin-2-yl)-3-methyl-1H-pyrazol-5-yl)furan-2-carboxamide (**8**). Furan-2-carboxylic acid (0.031 g, 0.27 mmol, 3 eq) and DIPEA (0.050 g, 0.38 mmol, 4.2 eq) were dissolved in DMF (0.9 mL) and allowed to stir at room temperature for 10 minutes. Next, 2-(3H-[1,2,3]triazolo[4,5-b]pyridin-3-yl)-1,1,3,3-tetramethylisouronium hexafluorophosphate(V) (0.11 g, 0.29 mmol, 3.2 eq) was added to the vial. This solution was allowed to stir for 1 hour at room temperature. After 1 hour intermediate **5** (0.020 g, 0.091 mmol, 1 eq) was added and the solution was brought to 85 °C then stirred for 18 hours. Work-up was the same as general procedure A, yielding **8** as a white solid (0.003 g, 0.009 mmol, 10%). ^{1}H NMR (800 MHz, CDCl3) δ 12.51 (s, 1H), 10.27 (s, 1H), 7.56 (d, J = 1.7 Hz, 1H), 7.33 (d, J = 3.5 Hz, 1H), 6.85 (s, 1H), 6.64 (dd, J = 3.5, 1.7 Hz, 1H), 6.12 (s, 1H), 2.71 (q, J = 7.6 Hz, 2H), 2.32 (s, 3H), 1.40 (t, J = 7.6 Hz, 3H). ^{13}C NMR (201 MHz, CDCl3) δ 168.4, 161.0, 154.3, 154.0, 148.5, 147.2, 144.7, 140.3, 116.4, 113.0, 107.8, 99.0, 30.6, 14.2, 12.2. APCI-MS(+): m/z 314.3 $[M+H]^+$. APCI-MS(-): m/z 312.1 $[M-H]^-$. HPLC retention time: 11.686 min. HPLC purity 97.9%.

N-(1-(6-Ethyl-4-oxo-1,4-dihydropyrimidin-2-yl)-3-methyl-1H-pyrazol-5-yl)picolinamide (**9**). Prepared using general procedure A with picolinic acid (0.037 g, 0.30 mmol, 1.3 eq), BTFFH (0.11 g, 0.34 mmol, 1.5 eq), DCM (0.5 mL), DIPEA (180 μL, 1.0 mmol, 4.3 eq), and **(5)** (0.0500 g, 0.23 mmol, 1 eq) to produce **9** (0.036 g, 0.11 mmol, 48%) as a tan solid. ^{1}H NMR (800 MHz, $CDCl_3$) δ 13.48 (s, 1H), 10.26 (s, 1H), 8.64 (ddd, J = 4.7, 1.7, 0.9 Hz, 1H), 8.28 (dt, J = 7.8, 1.1 Hz, 1H),

7.94 (td, J = 7.7, 1.7 Hz, 1H), 7.53 (ddd, J = 7.5, 4.7, 1.2 Hz, 1H), 6.93 (s, 1H), 6.11 (s, 1H), 2.77 (q, J = 7.6 Hz, 2H), 2.32 (s, 3H), 1.43 (t, J = 7.6 Hz, 3H). ^{13}C NMR (201 MHz, $CDCl_3$) δ 169.1, 161.9, 161.3, 153.8, 148.9, 148.3, 148.2, 140.6, 137.7, 127.0, 123.0, 107.7, 99.0, 30.7, 14.2, 12.3. APCI-MS(+): m/z 325.1 $[M+H]^+$. APCI-MS(-): m/z 323.0 $[M-H]^-$. HPLC retention time: 12.473 min. HPLC purity 95.1%.

N-(1-(6-Ethyl-4-oxo-1,4-dihydropyrimidin-2-yl)-3-methyl-1H-pyrazol-5-yl)-3-fluorobenzamide (**10**)**.** Prepared using general procedure A with 3-fluorobenzoic acid (0.046 g, 0.30 mmol,1.3 eq), BTFFH (0.11 g, 0.34 mmol, 1.5 eq), DCM (440 µL), DIPEA (180 µL, 1.0 mmol, 4.3. eq), and **5** (0.050 g, 0.23 mmol, 1 eq). Required additional purification via normal phase flash chromatography (DCM:MeOH, 10% MeOH isocratic) to produce **10** (0.009 g, 0.003 mmol, 11%) as a white solid. ^{1}H NMR (800 MHz, $CDCl_3$) δ 12.43 (s, 1H), 10.29 (s, 1H), 7.78 (d, J = 7.7 Hz, 1H), 7.68 (dt, J = 9.2, 1.9 Hz, 1H), 7.52 (td, J = 8.0, 5.4 Hz, 1H), 7.32 (td, J = 8.2, 2.6 Hz, 1H), 6.88 (s, 1H), 6.11 (s, 1H), 2.67 (q, J = 7.5 Hz, 2H), 2.32 (s, 3H), 1.30 (t, J = 7.6 Hz, 3H). ^{13}C NMR (201 MHz, $CDCl_3$) δ 167.9, 162.9 (d, ^{1}J = 248.5 Hz), 162.1, 160.8, 154.2, 148.8, 140.8, 135.5 (d, ^{3}J = 7.1 Hz), 130.7 (d, ^{3}J = 7.9 Hz), 123.0, 119.8 (d, ^{2}J = 21.1 Hz), 114.5 (d, ^{2}J = 23.1 Hz), 107.8, 99.2, 30.7, 14.2, 12.3. APCI-MS(+): 342.1 $[M+H]^+$. APCI-MS(-): 340.0 $[M-H]^-$. HPLC retention time: 12.844 min. HPLC purity 99.1%.

N-(1-(6-Ethyl-4-oxo-1,4-dihydropyrimidin-2-yl)-3-methyl-1H-pyrazol-5-yl)-4-fluorobenzamide (**11**). Prepared using general procedure A with 4-fluorobenzoic acid (0.046 g, 0.30 mmol, 1.3 eq), BTFFH (0.11 g, 0.34 mmol, 1.5 eq), DCM (0.5 mL), DIPEA (180 µL, 1.0 mmol, 4.3 eq), and **5** (0.050 g, 0.23 mmol, 1 eq) to produce **11** (0.020 g, 0.057 mmol, 25%) as a white solid. ^{1}H NMR (800 MHz, $CDCl_3$) δ 12.35 (s, 1H), 10.30 (s, 1H), 8.01 – 7.98 (m, 2H), 7.23 – 7.19 (m, 2H), 6.87 (s, 1H), 6.11 (s, 1H), 2.64 (q, J = 7.6 Hz, 2H), 2.31 (s, 3H), 1.30 (t, J = 7.5 Hz, 3H). ^{13}C NMR (201

MHz, $CDCl_3$) δ 167.8, 165.5 (d, ^1J = 254.5 Hz), 162.4, 160.8, 154.2, 148.8, 141.0, 129.7 (d, ^3J = 9.1 Hz), 129.5, 116.1 (d, ^2J = 22.1 Hz), 107.8, 99.0, 30.7, 14.2, 12.3. APCI-MS(+): 342.1 $[M+H]^+$. APCI-MS(-): 340.0 $[M-H]^-$. HPLC retention time: 12.722 min. HPLC purity 99.1%.

N-(1-(6-Ethyl-4-oxo-1,4-dihydropyrimidin-2-yl)-3-methyl-1H-pyrazol-5-yl)-3-chlorobenzamide (**12**). Prepared using general procedure A with 3-chlorobenzoic acid (0.046 g, 0.30 mmol, 1.3 eq), BTFFH (0.11 g, 0.34 mmol, 1.5 eq), DCM (0.5 mL), DIPEA (180 µL, 1.0 mmol, 4.3 eq), and **5** (0.050 g, 0.23 mmol, 1 ew) to produce **12** (0.019 g, 0.053 mmol, 23%) as a white solid. ^1H NMR (800 MHz, $CDCl_3$) δ 12.45 (s, 1H), 10.30 (s, 1H), 7.93 – 7.90 (m, 2H), 7.59 (d, J = 8.0 Hz, 1H), 7.49 (t, J = 7.8 Hz, 1H), 6.88 (s, 1H), 6.11 (s, 1H), 2.70 (q, J = 7.5 Hz, 2H), 2.32 (s, 3H), 1.30 (t, J = 7.5 Hz, 3H). ^{13}C NMR (201 MHz, $CDCl_3$) δ 168.0, 162.0, 160.8, 154.1, 148.8, 140.8, 135.1, 134.9, 132.7, 130.4, 127.0, 125.9, 107.8, 99.2, 30.7, 14.2, 12.3. APCI-MS(+): m/z 360.1, 358.1 $[M+H]^+$. APCI-MS(-): m/z 357.9, 355.9 $[M-H]^-$. HPLC retention time: 13.470 min. HPLC purity 98.1%.

N-(1-(6-Ethyl-4-oxo-1,4-dihydropyrimidin-2-yl)-3-methyl-1H-pyrazol-5-yl)-4-chlorobenzamide (**13**). Prepared using general procedure A with 4-chlorobenzoic acid (0.046 g, 0.30 mmol, 1.3 eq), BTFFH (0.11 g, 0.34 mmol, 1.5 eq), DCM (0.5 mL), DIPEA (180 µL, 1.0 mmol, 4.3 eq), and **5** (0.050 g, 0.23 mmol, 1 eq) to produce **13** (0.027 g, 0.075 mmol, 33%) as a white solid. ^1H NMR (800 MHz, $CDCl_3$) δ 12.38 (s, 1H), 10.30 (s, 1H), 7.92 (dt, J = 8.7, 2.0 Hz, 2H), 7.51 (dt, J = 8.7, 2.0 Hz, 2H), 6.87 (s, 1H), 6.11 (s, 1H), 2.64 (q, J = 7.5 Hz, 2H), 2.31 (s, 3H), 1.30 (t, J = 7.5 Hz, 3H). ^{13}C NMR (201 MHz, $CDCl_3$) δ 167.8, 162.4, 160.8, 154.2, 148.8, 140.9, 139.2, 131.6, 129.2,

128.7, 107.8, 99.1, 30.7, 14.2, 12.3. APCI-MS(+): m/z 360.1, 358.1 $[M+H]^+$. APCI-MS(-): m/z 358.0, 355.9 $[M-H]^-$. HPLC retention time: 13.357 min. HPLC purity 100%.

N-(1-(6-Ethyl-4-oxo-1,4-dihydropyrimidin-2-yl)-3-methyl-1H-pyrazol-5-yl)-2-methylbenzamide (**15**). Prepared using general procedure A with 2-methylbenzoic acid (0.040 g, 0.30 mmol, 1.3 eq), BTFFH (0.11 g, 0.34 mmol, 1.5 eq), DCM (0.5 mL), DIPEA (180 μL, 1.0 mmol, 4.3 eq), and **5** (0.050 g, 0.23 mmol) to produce **15** (0.006 g, 0.02 mmol, 8%) as a white solid. ^{1}H NMR (800 MHz, $CDCl_3$) δ 12.01 (s, 1H), 10.27 (s, 1H), 7.62 (d, J = 7.6 Hz, 1H), 7.42 (t, J = 7.5 Hz, 1H), 7.32 (d, J = 7.6 Hz, 1H), 7.29 (t, J = 7.5 Hz, 1H), 6.89 (s, 1H), 6.05 (s, 1H), 2.58 (s, 3H), 2.46 (q, J = 7.5 Hz, 2H), 2.31 (s, 3H), 1.10 (t, J = 7.6 Hz, 3H). ^{13}C NMR (201 MHz, $CDCl_3$) δ 168.1, 165.7, 160.9, 154.1, 148.6, 141.0, 138.2, 134.2, 131.9, 131.3, 126.8, 125.9, 107.7, 98.8, 30.3, 20.4, 14.2, 11.9. APCI-MS(+): m/z 338.2 $[M+H]^+$. APCI-MS(-): m/z 336.1 $[M-H]^-$. HPLC retention time: 12.897 min. HPLC purity 97.5%.

N-(1-(6-Ethyl-4-oxo-1,4-dihydropyrimidin-2-yl)-3-methyl-1H-pyrazol-5-yl)-3-methylbenzamide (**16**). Prepared using general procedure A with 3-methylbenzoic acid (0.040 g, 0.30 mmol, 1.3 eq), BTFFH (0.11 g, 0.34 mmol, 1.5 eq), DCM (0.5 mL), DIPEA (180 μL, 1.0 mmol), and **5** (0.050 g, 0.23 mmol) to produce **16** (0.015 g, 0.044 mmol, 19%) as a white solid. ^{1}H NMR (800 MHz, $CDCl_3$) δ 12.30 (s, 1H), 10.32 (s, 1H), 7.80 – 7.77 (m, 2H), 7.43 – 7.40 (m, 2H), 6.89 (s, 1H), 6.10 (s, 1H), 2.67 (q, J = 7.5 Hz, 2H), 2.46 (s, 3H), 2.31 (s, 3H), 1.29 (t, J = 7.6 Hz, 3H). ^{13}C NMR (201 MHz, $CDCl_3$) δ 168.0, 163.7, 160.9, 154.2, 148.7, 141.2, 138.8, 133.5, 133.2, 128.8, 127.8, 124.6, 107.7, 99.0, 30.7, 21.3, 14.2, 12.3. APCI-MS(+): m/z 338.2 $[M+H]^+$. APCI-MS(-): m/z 336.1 $[M-H]^-$. HPLC retention time: 13.084 min. HPLC purity 96.6%.

N-(1-(6-Ethyl-4-oxo-1,4-dihydropyrimidin-2-yl)-3-methyl-1H-pyrazol-5-yl)-4-methylbenzamide (**17**). Prepared using general procedure A with 4-methylbenzoic acid (0.040 g, 0.30 mmol, 1.3 eq), BTFFH (0.11 g, 0.34 mmol, 1.3 eq), DCM (0.5 mL), DIPEA (180 μL, 1.0 mmol, 4.3 eq), and **5** (0.050 g, 0.23 mmol) to produce **17** (0.033 g, 0.097 mmol, 43%) as a white solid. ^{1}H NMR (800 MHz, $CDCl_3$) δ 12.31 (s, 1H), 10.31 (s, 1H), 7.87 (d, J = 8.3 Hz, 2H), 7.32 (d, J = 8.3 Hz, 2H), 6.87 (s, 1H), 6.10 (s, 1H), 2.66 (q, J = 7.6 Hz, 2H), 2.45 (s, 3H), 2.31 (s, 3H), 1.31 (t, J = 7.6 Hz, 3H). ^{13}C NMR (201 MHz, $CDCl_3$) δ 168.1, 163.5, 160.9, 154.2, 148.8, 143.5, 141.2, 130.4, 129.6, 127.3, 107.6, 98.9, 30.7, 21.6, 14.2, 12.3. APCI-MS(+): m/z 338.2 $[M+H]^+$. APCI-MS(-): m/z 336.0 $[M-H]^-$. HPLC retention time: 13.039 min. HPLC purity 96.6%.

N-(1-(4-Ethyl-6-oxo-1,6-dihydropyrimidin-2-yl)-3-methyl-1H-pyrazol-5-yl)-3-(trifluoromethyl) benzamide (**18**). Prepared using general procedure A with 3-(trifluoromethyl)benzoic acid (0.056 g, 0.30 mmol, 1.3 eq), BTFFH (0.11 g, 0.34 mmol, 1.5 eq), DCM (0.5 mL), DIPEA (180 μL, 1.0 mmol, 4.3 eq), and **5** (0.050 g, 0.23 mmol, 1 eq) to produce **18** (0.021 g, 0.052 mmol, 23%) as a white solid. ^{1}H NMR (800 MHz, $CDCl_3$) δ 12.45 (s, 1H), 10.31 (s, 1H), 8.22 (d, J = 7.8 Hz, 1H), 8.18 (s, 1H), 7.89 (d, J = 7.8 Hz, 1H), 7.70 (t, J = 7.8 Hz, 1H), 6.92 (s, 1H), 6.11 (s, 1H), 2.65 (q, J = 7.7 Hz, 2H), 2.33 (d, J = 2.6 Hz, 3H), 1.25 (t, J = 7.5 Hz, 3H). ^{13}C NMR (201 MHz, $CDCl_3$) δ 168.0, 162.0, 160.8, 154.1, 148.7, 140.7, 134.1, 131.5 (q, ^{2}J = 33.0 Hz), 131.2, 129.7, 129.3, 123.7, 123.6 (q, ^{1}J = 271.0 Hz), 107.7, 99.5, 30.6, 14.2, 12.1. APCI-MS(+): m/z 392.2 $[M+H]^+$, 252.1, 220.1. APCI-MS(-): m/z 390.0 $[M-H]^-$. HPLC retention time: 13.454 min. HPLC purity 96.5%.

N-(1-(6-Ethyl-4-oxo-1,4-dihydropyrimidin-2-yl)-3-methyl-1H-pyrazol-5-yl)-2ethylbenzamide (**19**). Prepared using general procedure A with 2-ethylbenzoic acid (0.045 g, 0.30 mmol, 1.3 eq), BTFFH (0.11 g, 0.34 mmol, 1.5 eq), DCM (0.5 mL), DIPEA (180 μL, 1.0 mmol, 4.3 eq), and **5** (0.050 g, 0.23 mmol, 1 eq) to produce **19** (0.004 g, 0.012 mmol, 5%) as a white solid. ^{1}H NMR

(800 MHz, $CDCl_3$) δ 11.99 (s, 1H), 10.28 (s, 1H), 7.58 (d, J = 7.6 Hz, 1H), 7.46 (t, J = 7.6 Hz, 1H), 7.35 (d, J = 7.6 Hz, 1H), 7.28 (t, J = 7.5 Hz, 1H), 6.89 (s, 1H), 6.04 (s, 1H), 2.93 (q, J = 7.5 Hz, 2H), 2.43 (q, J = 7.7 Hz, 2H), 2.31 (s, 3H), 1.27 (t, J = 7.5 Hz, 3H), 1.06 (t, J = 7.6 Hz, 3H). ^{13}C NMR (201 MHz, $CDCl_3$) δ 168.1, 165.8, 161.0, 154.1, 148.6, 144.2, 141.0, 134.1, 131.3, 130.3, 126.8, 125.9, 107.7, 98.8, 30.3, 26.6, 16.0, 14.2, 11.8. APCI-MS(+): m/z 352.2 $[M+H]^+$. APCI-MS(-): m/z 350.1 $[M-H]^+$. HPLC retention time: 8.823 min (elution was 9 min gradient + 3 min 95% hold). HPLC purity 96.3%.

N-(1-(6-Ethyl-4-oxo-1,4-dihydropyrimidin-2-yl)-3-methyl-1H-pyrazol-5-yl)-3-ethylbenzamide (**20**). Prepared using general procedure A with 3-ethylbenzoic acid (0.045 g, 0.30 mmol, 1.3 eq), BTFFH (0.11 g, 0.34 mmol, 1.5 eq), DCM (0.5 mL), DIPEA (180 µL, 1.0 mmol, 4.3 eq), and **5** (0.050 g, 0.23 mmol, 1 eq) to produce **20** (0.009 g, 0.024 mmol, 11%) as a white solid. ^1H NMR (800 MHz, $CDCl_3$) δ 12.29 (s, 1H), 10.32 (s, 1H), 7.81 (s, 1H), 7.78 (dt, J = 6.9, 1.9 Hz, 1H), 7.46 – 7.43 (m, 2H), 6.90 (s, 1H), 6.10 (s, 1H), 2.75 (q, J = 7.7 Hz, 2H), 2.66 (q, J = 7.6 Hz, 2H), 2.31 (s, 3H), 1.30 (t, J = 7.8 Hz, 3H), 1.28 (t, J = 7.7 Hz, 3H). ^{13}C NMR (201 MHz, $CDCl_3$) δ 168.0, 163.8, 160.9, 154.2, 148.7, 145.3, 141.2, 133.3, 132.3, 128.9, 127.0, 124.6, 107.6, 99.0, 30.7, 28.9, 15.6, 14.2, 12.3. APCI-MS(+): m/z 352.2 $[M+H]^+$. APCI-MS(-): m/z 350.1 $[M-H]^-$. HPLC retention time: 13.557 min. HPLC purity 95.8%.

N-(1-(6-Ethyl-4-oxo-1,4-dihydropyrimidin-2-yl)-3-methyl-1H-pyrazol-5-yl)-4-ethylbenzamide (**21**). Prepared using general procedure A with 4-ethylbenzoic acid (0.045 g, 0.30 mmol, 1.3 eq), BTFFH (0.11 g, 0.34 mmol, 1.5 eq), DCM (0.5 mL), DIPEA (180 µL, 1.0 mmol, 4.3 eq), and **5** (0.050 g, 0.23 mmol, 1 eq) to produce **21** (0.020 g, 0.057 mmol, 25%) as a white solid. ^1H NMR (800 MHz, $CDCl_3$) δ 12.31 (s, 1H), 10.31 (s, 1H), 7.90 (d, J = 8.2 Hz, 2H), 7.35 (d, J = 8.0 Hz, 2H), 6.88 (s, 1H), 6.10 (s, 1H), 2.75 (q, J = 7.7 Hz, 2H), 2.67 (q, J = 7.5 Hz, 2H), 2.31 (s, 3H), 1.31

(t, J = 7.6 Hz, 3H), 1.29 (t, J = 7.7 Hz, 3H). ^{13}C NMR (201 MHz, CDCl3) δ 168.1, 163.5, 160.9, 154.2, 149.7, 148.8, 141.3, 130.6, 128.4, 127.4, 107.7, 98.9, 30.7, 28.9, 15.2, 14.2, 12.3. APCI-MS(+): m/z 352.2 $[M+H]^+$. APCI-MS(-): m/z 350.1 $[M-H]^-$. HPLC retention time: 13.531 min. HPLC purity 95.3%.

N-(1-(6-Ethyl-4-oxo-1,4-dihydropyrimidin-2-yl)-3-methyl-1H-pyrazol-5-yl)-3-isopropyl benzamide (**22**). Prepared using general procedure A with 3-isopropylbenzoic acid (0.049 g, 0.30 mmol, 1.3 eq), BTFFH (0.11 g, 0.34 mmol, 1.5 eq), DCM (0.5 mL), DIPEA (180 μL, 1.0 mmol, 4.3 eq), and **5** (0.050 g, 0.23 mmol, 1 eq) to produce **22** (0.003 g, 0.009 mmol, 4%) as a white solid. ^{1}H NMR (800 MHz, $CDCl_3$) δ 12.27 (s, 1H), 10.31 (s, 1H), 7.86 (s, 1H), 7.76 (d, J = 7.7 Hz, 1H), 7.49 (d, J = 7.5 Hz, 1H), 7.44 (t, J = 7.6 Hz, 1H), 6.90 (s, 1H), 6.10 (s, 1H), 3.00 (hept, J = 7.0 Hz, 1H), 2.66 (q, J = 7.5 Hz, 2H), 2.32 (s, 3H), 1.31 (d, J = 6.9 Hz, 6H), 1.28 (t, J = 7.6 Hz, 3H). ^{13}C NMR (201 MHz, $CDCl_3$) δ 168.1, 163.9, 160.9, 154.1, 150.1, 148.7, 141.2, 133.3, 130.7, 128.8, 126.1, 124.4, 107.6, 99.0, 34.3, 30.7, 23.9, 14.2, 12.3. APCI-MS(+): m/z 366.2 $[M+H]^+$. APCI-MS(-): m/z 364.1 $[M-H]^-$. HPLC retention time: 13.911 min. HPLC purity 95.9%.

N-(1-(4-Ethyl-6-oxo-1,6-dihydropyrimidin-2-yl)-3-methyl-1H-pyrazol-5-yl)-3-cyclopropylbenzamide (**23**). Prepared using general procedure B using 3-cyclopropylbenzoic acid (0.048 g, 0.30 mmol, 1.3 eq), BTFFH (0.11 g, 0.34 mmol, 1.5 eq), **5** (0.050 g, 0.23 mmol, 1 eq), DIPEA (100 μL, 0.57 mmol, 2.5 eq), LiHMDS 1.0 M in THF (1.03 mL, 1.03 mmol, 4.5 eq), and DCM (0.5 mL) to produce **23** (0.013 g, 0.035 mmol, 15%). ^{1}H NMR (800 MHz, $CDCl_3$) δ 12.29 (s, 1H), 10.25 (s, 1H), 7.75 (s, 1H), 7.71 (d, J = 7.6 Hz, 1H), 7.39 (t, J = 7.7 Hz, 1H), 7.27 (d, J = 7.7 Hz, 1H), 6.89 (s, 1H), 6.10 (s, 1H), 2.67 (q, J = 7.6 Hz, 2H), 2.31 (s, 3H), 2.01 – 1.96 (m, 1H),

1.28 (t, J = 7.6 Hz, 3H), 1.06 – 1.02 (m, 2H), 0.80 – 0.77 (m, 2H). ^{13}C NMR (201 MHz, $CDCl_3$) δ 168.1, 163.8, 160.9, 154.1, 148.7, 145.3, 141.1, 133.2, 129.7, 128.7, 125.6, 124.0, 107.6, 99.0, 30.7, 15.4, 14.2, 12.3, 9.4. APCI-MS(+): m/z 364.1 $[M+H]^+$. APCI-MS(-): m/z 361.9 $[M-H]^-$. HPLC retention time: 13.449 min. HPLC purity 95.7%.

N-(1-(4-Ethyl-6-oxo-1,6-dihydropyrimidin-2-yl)-3-methyl-1H-pyrazol-5-yl)-3-tert-butylbenzamide (**24**). Prepared using general procedure B using 3-*tert*-butylbenzoic acid (0.053 g, 0.30 mmol, 1.3 eq), BTFFH (0.11 g, 0.34 mmol, 1.5 eq), **5** (0.050 g, 0.23 mmol, 1 eq), DIPEA (100 µL, 0.57 mmol, 2.5 eq), LiHMDS 1.0 M in THF (1.03 mL, 1.03 mmol, 4.5 eq), and DCM (0.5 mL) to produce **24** an off-white powder (0.009 g, 0.022 mmol, 10%). ^{1}H NMR (800 MHz, $CDCl_3$) δ 12.24 (s, 1H), 10.26 (s, 1H), 8.09 (s, 1H), 7.68 (d, J = 7.7 Hz, 1H), 7.64 (d, J = 7.8 Hz, 1H), 7.43 (t, J = 7.7 Hz, 1H), 6.90 (s, 1H), 6.10 (s, 1H), 2.64 (q, J = 7.6 Hz, 2H), 2.32 (s, 3H), 1.38 (s, 9H), 1.27 (t, J = 7.6 Hz, 3H). ^{13}C NMR (201 MHz, $CDCl_3$) δ 168.1, 164.2, 160.9, 154.1, 152.6, 148.7, 141.2, 133.1, 129.9, 128.3, 125.4, 123.3, 107.6, 99.0, 35.0, 31.2, 30.7, 14.2, 12.2. APCI-MS(+): m/z 380.0 $[M+H]^+$. APCI-MS(-): m/z 378.0 $[M-H]^-$. HPLC retention time: 14.111 min. HPLC purity 98.7%.

N-(1-(4-Ethyl-6-oxo-1,6-dihydropyrimidin-2-yl)-3-methyl-1H-pyrazol-5-yl)-4-tert-butylbenzamide (**25**). Prepared using general procedure B using 4-tert-butylbenzoic acid (0.053 g, 0.30 mmol, 1.3 eq), BTFFH (0.11 g, 0.34 mmol, 1.5 eq), **5** (0.05 g, 0.23 mmol, 1 eq), DIPEA (100 µL, 0.57 mmol, 2.5 eq), LiHMDS 1.0 M in THF (1.03 mL, 1.03 mmol, 4.5 eq), and DCM (0.5 mL) to produce **25** an off-white powder (0.021 g, 0.056 mmol, 25%). ^{1}H NMR (800 MHz, $CDCl_3$) δ 12.30 (s, 1H), 10.30 (s, 1H), 7.92 (d, J = 8.0 Hz, 2H), 7.53 (d, J = 8.0 Hz, 2H), 6.89 (s, 1H), 6.11 (s, 1H), 2.68 (q, J = 7.5 Hz, 2H), 2.31 (s, 3H), 1.37 (s, 9H), 1.32 (t, J = 7.5 Hz, 3H). ^{13}C NMR (201 MHz, $CDCl_3$) δ 168.1, 163.4, 161.0, 156.6, 154.2, 148.8, 141.2, 130.3, 127.2, 125.8, 107.7, 98.9,

35.1, 31.1, 30.7, 14.2, 12.3. APCI-MS(+): m/z 380.1 [M+H], 338.1, 299.0, 240.1, 220.0, 161.0. APCI-MS(-): m/z 377.9 [M-H]. HPLC retention time: 14.124 min. HPLC purity 97.8%.

N-(1-(4-Ethyl-6-oxo-1,6-dihydropyrimidin-2-yl)-3-methyl-1H-pyrazol-5-yl)-[1,1'-biphenyl]-3-carboxamide (**26**). Prepared using general procedure B using biphenyl-3-carboxylic acid (0.059 g, 0.30 mmol, 1.3 eq), BTFFH (0.11 g, 0.34 mmol, 1.5 eq), **5** (0.050 g, 0.23 mmol, 1 eq), DIPEA (100 µL, 0.57 mmol, 2.5 eq), LiHMDS 1.0 M in THF (1.03 mL, 1.03 mmol, 4.5 eq), and DCM (0.5 mL) to produce **26** as an off-white powder (0.021 g, 0.053 mmol, 23%). ^{1}H NMR (800 MHz, CDCl3) δ 12.41 (s, 1H), 10.29 (s, 1H), 8.15 (s, 1H), 7.97 (d, J = 7.6 Hz, 1H), 7.81 (d, J = 7.8 Hz, 1H), 7.62 – 7.59 (m, 3H), 7.48 (t, J = 7.5 Hz, 2H), 7.42 (t, J = 7.2 Hz, 1H), 6.92 (s, 1H), 6.04 (s, 1H), 2.43 (q, J = 7.5 Hz, 2H), 2.32 (s, 3H), 1.03 (t, J = 7.5 Hz, 3H). ^{13}C NMR (201 MHz, CDCl3) δ 168.1, 163.5, 160.9, 154.1, 148.7, 142.5, 141.1, 140.1, 133.8, 131.5, 129.4, 129.0, 128.0, 127.3, 126.1, 126.1, 107.5, 99.1, 30.6, 14.2, 11.9. APCI-MS(+): m/z 400.0 $[M+H]^{+}$. APCI-MS(-): m/z 397.9 $[M-H]^{-}$. HPLC retention time: 13.921 min. HPLC purity 98.4%.

N-(1-(4-Ethyl-6-oxo-1,6-dihydropyrimidin-2-yl)-3-methyl-1H-pyrazol-5-yl)-[1,1'-biphenyl]-4-carboxamide (**27**). Prepared using general procedure B using biphenyl-4-carboxylic acid (0.059 g, 0.30 mmol, 1.3 eq), BTFFH (0.11 g, 0.34 mmol, 1.5 eq), **5** (0.050 g, 0.23 mmol, 1 eq), DIPEA (100 µL, 0.57 mmol, 2.5 eq), LiHMDS 1.0 M in THF (1.03 mL, 1.03 mmol, 4.5 eq), and DCM (0.5 mL) to produce **27** as an off-white powder (0.045 g, 0.11 mmol, 49%). ^{1}H NMR (800 MHz, CDCl3) δ 12.41 (s, 1H), 10.30 (s, 1H), 8.05 (d, J = 7.9 Hz, 2H), 7.74 (d, J = 7.9 Hz, 2H), 7.65 (d, J = 7.8 Hz, 2H), 7.50 (t, J = 7.5 Hz, 2H), 7.43 (t, J = 7.5 Hz, 1H), 6.91 (s, 1H), 6.11 (s, 1H), 2.69 (q, J = 7.5 Hz, 2H), 2.32 (s, 3H), 1.32 (t, J = 7.5 Hz, 3H). ^{13}C NMR (201 MHz, CDCl3) δ 168.0, 163.3, 160.9, 154.2, 148.8, 145.6, 141.2, 139.6, 131.8, 129.0, 128.4, 127.9, 127.5, 127.3, 107.7,

99.0, 30.7, 14.2, 12.3. APCI-MS(+): m/z 400.0 $[M+H]^+$. APCI-MS(-): m/z 397.9 $[M-H]^-$. HPLC retention time: 13.911 min. HPLC purity 99.4%

N-(1-(6-Ethyl-4-oxo-1,4-dihydropyrimidin-2-yl)-3-methyl-1H-pyrazol-5-yl)-3-methoxybenzamide (**28**). Prepared using general procedure A with 3-methoxybenzoic acid (0.045 g, 0.30 mmol, 1.3 eq), BTFFH (0.1080 g, 0.3416 mmol, 1.5 eq), DCM (0.5 mL), DIPEA (180 μL, 1.0 mmol, 4.3 eq), and **5** (0.0500 g, 0.228 mmol, 1 eq) to produce **28** (0.028 g, 0.078 mmol, 34%) as a white solid. ^{1}H NMR (800 MHz, $CDCl_3$) δ 12.34 (s, 1H), 10.33 (s, 1H), 7.54 (s, 1H), 7.49 (d, J = 7.7 Hz, 1H), 7.41 (t, J = 7.9 Hz, 1H), 7.13 (d, J = 8.3 Hz, 1H), 6.86 (s, 1H), 6.09 (s, 1H), 3.88 (s, 3H), 2.65 (q, J = 7.6 Hz, 2H), 2.30 (s, 3H), 1.28 (t, J = 7.6 Hz, 3H). ^{13}C NMR (201 MHz, $CDCl_3$) δ 168.1, 163.3, 160.9, 160.2, 154.1, 148.7, 141.1, 134.6, 129.8, 118.8, 118.3, 113.4, 107.7, 98.9, 55.6, 30.6, 14.2, 12.3. APCI-MS(+): m/z 354.1 $[M+H]^+$. APCI-MS(-): m/z 352.0 $[M-H]^-$. HPLC retention time: 12.600 min. HPLC purity 99.2%.

N-(1-(6-Ethyl-4-oxo-1,4-dihydropyrimidin-2-yl)-3-methyl-1H-pyrazol-5-yl)-4-methoxybenzamide (**29**). Prepared using general procedure A with 4-methoxybenzoic acid (0.045 g, 0.30 mmol, 1.3 eq), BTFFH (0.11 g, 0.34 mmol, 1.5 eq), DCM (0.5 mL), DIPEA (180 μL, 1.0 mmol, 4.3 eq), and **5** (0.050 g, 0.23 mmol, 1 eq) to produce **29** (0.029 g, 0.083 mmol, 36%) as a white solid. ^{1}H NMR (800 MHz, $CDCl_3$) δ 12.25 (s, 1H), 10.31 (s, 1H), 7.94 (d, J = 8.8 Hz, 2H), 7.00 (d, J = 8.9 Hz, 2H), 6.86 (s, 1H), 6.10 (s, 1H), 3.90 (s, 3H), 2.66 (q, J = 7.5 Hz, 2H), 2.30 (s, 3H), 1.31 (t, J = 7.6 Hz, 3H). ^{13}C NMR (201 MHz, $CDCl_3$) δ 168.0, 163.2, 163.1, 160.9, 154.2, 148.8, 141.4, 129.3, 125.5, 114.1, 107.6, 98.7, 55.6, 30.7, 14.2, 12.3. APCI-MS(+): m/z 354.2 $[M+H]^+$. APCI-MS(-): m/z 352.1 $[M-H]^-$. HPLC retention time: 12.451 min. HPLC purity 98.8%.

N-(1-(4-ethyl-6-oxo-1,6-dihydropyrimidin-2-yl)-3-methyl-1H-pyrazol-5-yl)-3-(methylthio) benzamide (**30**). Prepared using general procedure A with 3-(methylthio)benzoic acid (0.050 g, 0.30 mmol, 1.3 eq), BTFFH (0.1080 g, 0.3416 mmol, 1.5 eq), DCM (0.5 mL), DIPEA (180 µL, 1.0 mmol, 4.3 eq), and **5** (0.050 g, 0.23 mmol, 1 eq) to produce **30** (0.026 g, 0.072 mmol, 31%) as a white solid. ^{1}H NMR (800 MHz, $CDCl_3$) δ 12.37 (s, 1H), 10.30 (s, 1H), 7.86 (t, J = 1.8 Hz, 1H), 7.71 (dt, J = 7.4, 1.5 Hz, 1H), 7.46 (dt, J = 7.9, 1.5 Hz, 1H), 7.44 (t, J = 7.8 Hz, 1H), 6.88 (s, 1H), 6.10 (s, 1H), 2.69 (q, J = 7.5 Hz, 2H), 2.55 (s, 3H), 2.31 (s, 3H), 1.29 (t, J = 7.5 Hz, 3H). ^{13}C NMR (201 MHz, $CDCl_3$) δ 168.1, 163.1, 160.9, 154.1, 148.7, 141.0, 140.4, 133.8, 130.1, 129.2, 125.5, 123.6, 107.7, 99.1, 30.8, 15.8, 14.2, 12.3. APCI-MS(+): m/z 392.2 $[M+Na]^+$, 370.2 $[M+H]^+$. APCI-MS(-): m/z 390.0 $[M+Na-2H]^-$, 368.1 $[M-H]^-$. HPLC retention time: 13.222 min. HPLC purity 97.3%.

N-(1-(4-Ethyl-6-oxo-1,6-dihydropyrimidin-2-yl)-3-methyl-1H-pyrazol-5-yl)-3-ethoxybenzamide (**31**). Prepared using general procedure A using 3-ethoxybenzoic acid (0.049 g, 0.30 mmol, 1.3 eq), BTFFH (0.11 g, 0.34 mmol, 1.5 eq), DCM (0.5 mL), DIPEA (180 µL, 1.0 mmol, 4.3 eq), and **5** (0.050 g, 0.23 mmol, 1 eq) to produce **31** as an off-white powder (0.004 g, 0.01 mmol, 5%). ^{1}H NMR (800 MHz, $CDCl_3$) δ 12.38 (s, 1H), 10.31 (s, 1H), 7.55 (s, 1H), 7.52 (d, J = 7.2 Hz, 1H), 7.42 (t, J = 7.9 Hz, 1H), 7.13 (dd, J = 8.3, 2.5 Hz, 1H), 6.89 (s, 1H), 6.11 (s, 1H), 4.13 (q, J = 6.9 Hz, 2H), 2.69 (q, J = 7.6 Hz, 2H), 2.33 (s, 3H), 1.46 (t, J = 7.0 Hz, 3H), 1.30 (t, J = 7.5 Hz, 3H). ^{13}C NMR (201 MHz, $CDCl_3$) δ 168.1, 163.3, 160.9, 159.5, 154.0, 148.6, 141.0, 134.5, 129.7, 118.8, 118.6, 113.9, 107.6, 98.9, 63.7, 30.5, 14.7, 14.2, 12.2. APCI-MS(+): m/z 368.4 $[M+H]^+$. APCI-MS(-): m/z 366.3 $[M-H]^-$. HPLC retention time: 13.222 min. HPLC purity 97.1%.

N-(1-(6-Ethyl-4-oxo-1,4-dihydropyrimidin-2-yl)-3-methyl-1H-pyrazol-5-yl)-4-(methoxymethoxy) benzamide (**32**). Prepared using general procedure A with 4-(methoxymethoxy)benzoic acid

(0.054 g, 0.30 mmol, 1.3 eq), BTFFH (0.11 g, 0.34 mmol, 1.5 eq), DCM (0.5 mL), DIPEA (180 µL, 1.0 mmol, 4.3 eq), and **5** (0.050 g, 0.23 mmol, 1 eq) to produce **32** (0.015 g, 0.039 mmol, 17%) as a white solid. ^{1}H NMR (800 MHz, $CDCl_3$) δ 12.27 (s, 1H), 10.30 (s, 1H), 7.94 (d, J = 8.3 Hz, 2H), 7.14 (d, J = 8.5 Hz, 2H), 6.87 (s, 1H), 6.11 (s, 1H), 5.26 (s, 2H), 3.51 (s, 3H), 2.66 (q, J = 7.5 Hz, 2H), 2.30 (s, 3H), 1.31 (t, J = 7.5 Hz, 3H). ^{13}C NMR (201 MHz, $CDCl_3$) δ 168.1, 163.0, 160.8, 154.2, 148.8, 141.3, 129.2, 126.5, 116.1, 107.6, 98.8, 94.2, 56.3, 30.7, 29.7, 14.2 (d, J = 18.6 Hz), 12.3. APCI-MS(+): m/z 384.1 $[M+H]^+$. APCI-MS(-): m/z 382.0 $[M-H]^-$. HPLC retention time: 12.392 min. HPLC purity 97.6%.

N-(1-(6-Ethyl-4-oxo-1,4-dihydropyrimidin-2-yl)-3-methyl-1H-pyrazol-5-yl)-4-hydroxybenzamide (**33**). Compound **30** (0.015 g, 0.039 mmol) was dissolved in DCM (5 mL) and allowed to cool to 0°C in an ice water bath. To this solution, excess trifluoroacetic acid (TFA) was added. It was allowed to stir for 3 hours at 0°C. The solution was concentrated on rotavapor, resuspended with hexanes, then filtered to produce **33** as a white solid (0.006 g, 0.02 mmol, 40%). ^{1}H NMR (800 MHz, DMSO-d_6) δ 12.53 (s, 1H), 10.35 (s, 1H), 7.82 (d, J = 8.2 Hz, 2H), 6.93 (d, J = 8.3 Hz, 2H), 6.74 (s, 1H), 6.29 (s, 1H), 2.68 (q, J = 7.8 Hz, 2H), 2.26 (s, 3H), 1.20 (t, J = 7.6 Hz, 3H). ^{13}C NMR (201 MHz, DMSO-d_6) δ 162.8, 162.0, 151.9, 141.3, 129.7, 124.2, 116.0, 97.7, 30.2, 14.4, 12.9. APCI-MS(+): m/z 340.2 $[M+H]^+$. APCI-MS(-): m/z 452.0 $[M+TFA-H]^-$, 338.0 $[M-H]^-$. HPLC retention time: 10.822 min. HPLC purity 99.4%.

N-(1-(6-Ethyl-4-oxo-1,4-dihydropyrimidin-2-yl)-3-methyl-1H-pyrazol-5-yl)-4-(dimethylamino) benzamide (**34**). The procedure for **34** was modified from a previous literature protocol.[47] 4-(Dimethylamino)benzoic acid (0.057 g, 0.34 mmol, 1.5 eq) was added to a 0.5-2 mL microwave vial and sealed and then flushed repeatedly with argon. T3P (290 µL 50% w/w in MeCN, 0.46

mmol, 2 eq) and pyridine (0.072 g, 74 µL, 0.91 mmol, 4 eq) were then added sequentially, and the vial was heated to 60°C for one hour.

In a separate vial, **5** (0.050 g, 0.23 mmol, 1 eq) was dissolved in 1,1,1,3,3,3-hexafluoro-2-propanol (HFIP) (200 µL) and added dropwise to the first microwave vial. The mixture was then heated to 80°C for 24 hours. It was then cooled to room temperature and quenched with 1 mL of DI H_2O. The mixture was transferred to a separatory flask and diluted with 20 mL DCM and 20 mL 1% aqueous HCl. The organic layer was collected and the aqueous layer was again extracted with 20 mL DCM. The combined organic layers were then washed with saturated $NaHCO_3$ and brine sequentially. The organic layer was dried with $MgSO_4$, filtered, and concentrated on rotavap. The resultant film was resuspended with hexanes to remove residual DCM to yield powder. This powder was suspended with 1-2 mL EtOAc and filtered to produce **34** as an off-white powder (0.023 g, 0.062 mmol, 27%). ^{1}H NMR (800 MHz, $CDCl_3$) δ 12.11 (s, 1H), 10.31 (s, 1H), 7.86 (d, J = 8.9 Hz, 2H), 6.84 (s, 1H), 6.70 (d, J = 8.8 Hz, 2H), 6.09 (s, 1H), 3.08 (s, 6H), 2.69 (q, J = 7.5 Hz, 2H), 2.29 (s, 3H), 1.33 (t, J = 7.6 Hz, 3H). ^{13}C NMR (201 MHz, $CDCl_3$) δ 168.2, 163.6, 161.0, 154.2, 153.1, 148.8, 141.8, 129.0, 119.6, 111.0, 107.5, 98.3, 40.1, 30.7, 14.2, 12.4. APCI-MS(+): m/z 367.2 $[M+H]^+$. APCI-MS(-): m/z 365.1 $[M-H]^-$. HPLC retention time: 12.590 min. HPLC purity 96.2%.

N-(1-(6-Ethyl-4-oxo-1,4-dihydropyrimidin-2-yl)-3-methyl-1H-pyrazol-5-yl)-2-(2-fluorophenyl) acetamide (**35**). Procedure was adapted from previously reported literature.[47] 2-(2-fluorophenyl)acetic acid (0.053 g, 0.34 mmol, 1.5 eq) and DIPEA (0.16 mL, 0.91 mmol, 4 eq) were added to a thick-walled 0.5-2 mL Biotage microwave vial equipped with stirbar and the vial was sealed. The vial was then purged and flushed with Argon repeatedly. The vial was placed in a 90°C sandbath and T3P (320 uL 50% w/w in MeCN, 0.48 mmol, 2 eq) was added dropwise to the

stirring mixture. This mixture was allowed to stir for 1-2 hours at 90°C. In a separate vial, **5** (0.050 g, 0.23 mmol, 1 eq) was added and then dissolved in 200 uL of HFIP. This solution was then added dropwise to the sealed microwave vial. The vial was then allowed to stir at 90°C overnight.

The following morning, the vial was allowed to come to room temperature and then 1 mL of aqueous 10% potassium carbonate solution was added to the vial and briefly agitated. It was allowed to stir at room temperature for at least 1 hour at room temperature. It was then transferred to a separatory flask and diluted with 15 mL of 10% potassium carbonate solution. Two liquid-liquid extractions were performed with equal volumes of DCM. The organic layers were collected and combined and then washed twice with equal volumes (25-30 mL) of 1% HCl and then once with brine. The organic layer was then collected, dried with $MgSO_4$, filtered, and then concentrated on rotavapor yielding a colored powder, film, or clear liquid. This film was diluted with a small volume of DCM and injected onto flash column and then eluted with an ethyl acetate gradient in hexanes. Fractions identified via APCI MS were then collected and dried to produce **35** as a white powder (0.003 g, 7 μmol, 3%). ^{1}H NMR (800 MHz, $CDCl_3$) δ 11.55 (s, 1H), 10.23 (s, 1H), 7.40 (t, J = 7.7 Hz, 1H), 7.35 – 7.30 (m, 1H), 7.17 (t, J = 7.5 Hz, 1H), 7.11 (t, J = 9.1 Hz, 1H), 6.77 (s, 1H), 6.05 (s, 1H), 3.81 (s, 2H), 2.44 (q, J = 7.5 Hz, 2H), 2.26 (s, 3H), 1.24 (t, J = 7.4 Hz, 3H). ^{13}C NMR (201 MHz, $CDCl_3$) δ 168.3, 166.5, 160.9, 160.9 (d, ^{1}J = 246.2 Hz), 153.7, 148.3, 140.4, 131.5, 129.6 (d, ^{3}J = 8.1 Hz), 124.6 (d, ^{4}J = 3.5 Hz), 120.9 (d, ^{2}J = 15.7 Hz), 115.6 (d, ^{2}J = 21.6 Hz), 107.5, 99.3, 37.6, 30.1, 14.1, 12.0. APCI-MS(+): m/z 356.4 $[M+H]^+$. APCI-MS(-): m/z 354.3 $[M-H]^-$. HPLC retention time: 12.254 min. HPLC purity 97.6%.

N-(1-(6-Ethyl-4-oxo-1,4-dihydropyrimidin-2-yl)-3-methyl-1H-pyrazol-5-yl)-2-(m-tolyl)acetamide (**36**). Prepared using general procedure A using 2-(*m*-tolyl)acetic acid (0.045 g, 0.30 mmol, 1.3 eq), BTFFH (0.11 g, 0.34 mmol, 1.5 eq), DCM (0.5 mL), DIPEA (180 μL, 1.0 mmol, 4.3 eq), and

5 (0.050 g, 0.23 mmol, 1 eq). Instead of purification via filtration, product was purified via normal phase flash column with an ethyl acetate gradient in hexanes to produce **36** as an off-white powder (0.018 g, 0.051 mmol, 22%). ^{1}H NMR (800 MHz, $CDCl_3$) δ 11.35 (s, 1H), 10.19 (s, 1H), 7.25 (t, J = 7.5 Hz, 1H), 7.14 – 7.11 (m, 3H), 6.77 (s, 1H), 6.00 (s, 1H), 3.75 (s, 2H), 2.35 (s, 3H), 2.30 (q, J = 7.5 Hz, 2H), 2.25 (s, 3H), 1.19 (t, J = 7.5 Hz, 3H). ^{13}C NMR (201 MHz, $CDCl_3$) δ 168.3, 167.9, 161.0, 153.8, 148.4, 140.6, 138., 133.5, 130., 129.0, 128.5, 126.3, 107.4, 99.2, 44.9, 30.2, 21.4, 14.1, 12.1. APCI-MS(+): m/z 352.2 $[M+H]^+$. APCI-MS(-): m/z 350.1 $[M-H]^-$. HPLC retention time: 12.696 min. HPLC purity 99.4%.

N-(1-(4-Ethyl-6-oxo-1,6-dihydropyrimidin-2-yl)-3-methyl-1H-pyrazol-5-yl)-2-fluoro-3-methyl benzamide (**37**). Prepared using general procedure A using 2-fluoro-3-methylbenzoic acid (0.046 g, 0.30 mmol, 1.3 eq), BTFFH (0.11 g, 0.34 mmol, 1.5 eq), DCM (0.5 mL), DIPEA (180 μL, 1.0 mmol, 4.3 eq), and **5** (0.050 g, 0.23 mmol, 1 eq) to produce **37** as an off-white powder (0.023 g, 0.066 mmol, 29%). ^{1}H NMR (800 MHz, $CDCl_3$) δ 12.39 (d, J = 9.4 Hz, 1H), 10.32 (s, 1H), 7.95 (t, J = 7.6 Hz, 1H), 7.42 (t, J = 7.3 Hz, 1H), 7.21 (t, J = 7.6 Hz, 1H), 6.96 (s, 1H), 6.09 (s, 1H), 2.64 (q, J = 7.6 Hz, 2H), 2.37 (s, 3H), 2.30 (s, 3H), 1.25 (t, J = 7.5 Hz, 3H). ^{13}C NMR (201 MHz, $CDCl_3$) δ 169.0, 161.1, 160.1, 158.9 (d, ^{1}J = 248.9 Hz), 153.8, 148.3, 140.5, 135.8 (d, ^{3}J = 6.0 Hz), 129.8, 125.7 (d, ^{2}J = 19.1 Hz), 124.6 (d, ^{4}J = 3.9 Hz), 120.4 (d, ^{2}J = 12.4 Hz), 107.8, 100.1, 30.2, 14.4 (d, ^{3}J = 4.9 Hz), 14.2, 12.4. APCI-MS(+): m/z 356.1 $[M+H]^+$. APCI-MS(-): m/z 353.9 $[M-H]^-$. HPLC retention time: 13.345 min. HPLC purity 99.2%.

N-(1-(4-ethyl-6-oxo-1,6-dihydropyrimidin-2-yl)-3-methyl-1H-pyrazol-5-yl)-2-fluoro-5-methyl benzamide (**38**). Prepared using general procedure A using 2-fluoro-5-methylbenzoic acid (0.046 g, 0.30 mmol, 1.3 eq), BTFFH (0.11 g, 0.34 mmol, 1.5 eq), DCM (0.5 μL), DIPEA (180 μL, 1.0 mmol, 4.3 eq), and **5** (0.050 g, 0.23 mmol, 1 eq) to produce **38** as an off-white powder (0.025 g,

0.070 mmol, 31%). ^{1}H NMR (800 MHz, $CDCl_3$) δ 12.31 (d, J = 8.9 Hz, 1H), 10.31 (s, 1H), 7.92 (d, J = 7.4 Hz, 1H), 7.37 – 7.33 (m, 1H), 7.09 (dd, J = 11.5, 8.4 Hz, 1H), 6.96 (s, 1H), 6.08 (s, 1H), 2.63 (q, J = 7.6 Hz, 2H), 2.40 (s, 3H), 2.31 (s, 3H), 1.23 (t, J = 7.5 Hz, 3H). ^{13}C NMR (201 MHz, $CDCl_3$) δ 169.1, 161.2, 160.0, 158.7 (d, ^{1}J = 247.9 Hz), 153.7, 148.2, 140.4, 135.0 (d, ^{3}J = 8.8 Hz), 134.9 (d, ^{4}J = 3.2 Hz), 132.3, 120.0 (d, ^{3}J = 11.7 Hz), 116.0 (d, ^{2}J = 23.8 Hz), 107.6, 100.2, 30.1, 20.6, 14.2, 12.2. APCI-MS(+): m/z 355.8 $[M+H]^+$. APCI-MS(-): m/z 353.9 $[M-H]^-$. HPLC retention time: 13.356 min. HPLC purity 98.4%.

N-(1-(4-ethyl-6-oxo-1,6-dihydropyrimidin-2-yl)-3-methyl-1H-pyrazol-5-yl)-3,4-dimethyl benzamide (**39**). Prepared using general procedure B at triple-scale using 3,4-dimethylbenzoic acid (0.134 g, 0.890 mmol, 1.3 eq), BTFFH (0.325 g, 1.03 mmol, 1.5 eq), **5** (0.150 g, 0.684 mmol, 1 eq), DIPEA (300 µL, 1.70 mmol, 2.5 eq), LiHMDS 1.0 M in THF (3.079 mL, 3.079 mmol, 4.5 eq), and DCM (1.5 mL) to produce **39** as an off-white powder (0.12 g, 0.34 mmol, 49.0%). ^{1}H NMR (800 MHz, $CDCl_3$) δ 12.24 (s, 1H), 10.31 (s, 1H), 7.74 (s, 1H), 7.71 (d, J = 7.8 Hz, 1H), 7.28 (d, J = 7.4 Hz, 1H), 6.88 (s, 1H), 6.10 (s, 1H), 2.68 (q, J = 7.6 Hz, 2H), 2.36 (s, 6H), 2.31 (s, 3H), 1.30 (t, J = 7.6 Hz, 3H). ^{13}C NMR (201 MHz, $CDCl_3$) δ 168.1, 163.7, 160.9, 154.2, 148.7, 142.2, 141.3, 137.4, 130.7, 130.1, 128.4, 124.9, 107.6, 98.9, 30.7, 20.0, 19.8, 14.2, 12.3. APCI-MS(+): m/z 352.4 $[M+H]^+$. APCI-MS(-): m/z 350.3 $[M-H]^-$. HPLC retention time: 13.479 min. HPLC purity 100%.

N-(1-(4-ethyl-6-oxo-1,6-dihydropyrimidin-2-yl)-3-methyl-1H-pyrazol-5-yl)-3,5-dimethyl benzamide (**40**). Prepared using general procedure B using 3,5-dimethylbenzoic acid (0.045 g, 0.30 mmol, 1.3 eq), BTFFH (0.11 g, 0.34 mmol, 1.5 eq), **5** (0.050 g, 0.23 mmol, 1 eq), DIPEA (100 µL, 0.57 mmol, 2.5 eq), LiHMDS 1.0 M in THF (1.03 mL, 1.03 mmol, 4.5 eq), and DCM 0.5 mL to produce **40** as an off-white powder (0.019 g, 0.054 mmol, 24%). ^{1}H NMR (800 MHz, $CDCl_3$) δ

12.24 (s, 1H), 10.31 (s, 1H), 7.59 (s, 2H), 7.24 (s, 1H), 6.89 (s, 1H), 6.10 (s, 1H), 2.68 (q, J = 7.6 Hz, 2H), 2.41 (s, 6H), 2.31 (s, 3H), 1.29 (t, J = 7.5 Hz, 3H). ^{13}C NMR (201 MHz, $CDCl_3$) δ 168.0, 163.9, 160.9, 154.2, 148.7, 141.2, 138.7, 134.4, 133.1, 125.1, 107.6, 99.0, 30.8, 21.2, 14.2, 12.4. APCI-MS(+): m/z 352.4 $[M+H]^+$. APCI-MS(-): m/z 350.3 $[M-H]^-$. HPLC retention time: 13.614 min. HPLC purity 97.6%.

Biological Evaluation

High-throughput screen for AC1 inhibitors

The compound screen of the Life Chemicals diversity library was completed at the Biomolecular Screening and Drug Discovery Core Facility (BSDD), Purdue University (West Lafayette, IN). Cryopreserved HEK293 cells stably expressing AC1 (HEK-AC1) were washed with pre-warmed Opti-MEM from Thermo Fisher Scientific (Waltham) and centrifuged for 5 minutes at 150 x g. Supernatant was discarded and the cells were resuspended in Opti-MEM, counted, and plated into white opaque 384-well plates from Perkin Elmer (Waltham, MA). The plates were incubated for 1-hour in a 37°C incubator supplemented with 5% CO_2 to let the cells adhere to the plate prior compound addition. Subsequently, DMSO (negative control), the AC1 inhibitor ST034307 (positive control), or the Life Chemicals library compounds were added at a screening concentration of 10 μM using a pin tool liquid handling system. Following a 30-minute incubation at room temperature with DMSO or the compounds, the calcium ionophore, A23187, was added to all the wells to a final concentration of 3 μM in the presence of the phosphodiesterase inhibitor, 3-isobutyl-1-methylxanthine (IBMX). After 1-hour incubation with A23187 at room temperature, cAMP accumulation was measured using the HTRF cAMP kit from Cisbio (Bedford,

MA). The screen was carried out on three separate days and a total of 10,240 compounds were screened. The percentage inhibition (%) was calculated by normalizing the cAMP levels of each of the screen compounds to the mean cAMP levels of the positive control, ST034307, (100% inhibition) and DMSO (0% inhibition) in each plate.

Adenylyl cyclase cAMP accumulation assay

Cryopreserved HEK-ACΔ3/6 cells overexpressing human AC1, AC2, AC5 or AC8 were transferred to a 15-mL Falcon tube and gently resuspended in prewarmed Opti-MEM.[48] The cells were centrifuged for 5 minutes at 150 x g, supernatant was discarded, and the cell pellet was resuspended in 10 mL for a second centrifugation step. Then, the cells were counted, plated in a white opaque 384-well plate and incubated for 1-hour in a 37°C incubator supplemented with 5% CO_2. The hit compounds' working solutions were prepared in prewarmed Opti-MEM and successive serial dilutions were prepared using a Precision 2000 automated pipetting system. Dose response curves were generated for each hit compound using a three-fold serial dilution starting at 30 µM concentration (at least 6-points per curve). Compounds were added to the assay plates and incubated for 30 minutes at room temperature. AC activity was selectively stimulated on each AC isoform with 3 µM A23187 (AC1 and AC8), 100 nM PMA (AC2), or a low concentration (1 µM) of the AC activator, forskolin (AC5). All stimulants of AC activity were added in combination with IBMX at a final concentration of 0.5 mM. After 1-hour incubation with the stimulant at room temperature, cAMP accumulation was detected using the fluorescence-based Cisbio HTRF cAMP detection kit.

Thermodynamic solubility assay

The thermodynamic solubility of analogs was determined via an adapted protocol from literature.[53,54] Compounds were dissolved at a concentration of 0.5 mg/mL in DCM (minimum total volume 1.5 mL). 250 µL of this stock were transferred in triplicate to three separate HPLC vials equipped with stirbar, designated as experimental vials. A separate 200 µL was transferred to an additional HPLC vial for use as the standard. The DCM was then evaporated via gentle stirring on hotplate at 40°C for several hours. Vials marked as experimental were then diluted with 500 µL phosphate-buffered solution (pH 7.4), and the vial marked as standard was diluted with 500 µL DMSO. The vials were then stirred at room temperature for at least 24 hours. The stirbars were then removed and the vials were allowed to sit at room temperature for an additional 24 hours. The vials were then centrifuged to pellet undissolved compound and the supernatants were then injected on HPLC. Determination of thermodynamic solubility was then ascertained by comparing the integrated AUC of the standard vial compound peak (known concentration of 200 µg/mL) to the integration of the experimental vial compound peaks ($AUC_{exp.}/AUC_{std}= Conc._{exp}/Conc_{std}$ where $Conc._{exp}$= measured thermodynamic solubility).

Common neurological off-targets

Binding to common neurological off-targets was performed by the PDSP at the University of North Carolina at Chapel Hill. A complete protocol for all assays, including radiolabeled-tracers, K_i determinations, receptor binding profiles, and agonist and/or antagonist functional assay can be found online at the PDSP website (https://pdsp.unc.edu/pdspweb/content/UNC-CH%20Protocol%20Book.pdf).[74,75]

hERG binding assay

Radiometric displacement assay was performed by Eurofins Panlabs, LLC (New Taipei City, Taiwan) according to the published protocol[76] using [^{3}H]-astemizole.

Kinase binding assays

Radiometric phosphorylation assay was performed by Eurofins Panlabs, LLC (New Taipei City, Taiwan) against recombinant kinases in which labeling of substrate peptides with ^{33}P was quantified by scintillation counter. Procedures for each kinase are published online at eurofinsdiscoveryservices.com.

MDCK permeability assay

Assay and data analysis were performed by Eurofins Panlabs (MO, USA) according to the following protocol from Hidalgo et al.[77] using MDCKII cells and analysis was carried out as previously described.[78]

CYP Inhibition assay

Assay and data analysis were performed by Eurofins Panlabs (MO, USA) according the following protocol adapted from Stresser et al.[79]

Human Liver Microsome Stability

Assay and data analysis were performed by Eurofins Panlabs (MO, USA) according to the protocol from Obach et al.[80]

Evaluation of compound efficacy in CFA inflammatory pain model

Male and female C57BL/6N mice were obtained from Envigo (Indianapolis, IN). Mice (18-24g) were grouped and housed in plexiglass cages at ambient temperature (21-23°C) in normal (12 light:12 dark) light cycle (lights on at 7:00, lights off at 19:00). Water and food were provided *ad libitum*. All animal procedures were pre-approved by our Institutional Animal Care and Use Committee. For assessment of mechanical allodynia, mice were subjected to the CFA model and von Frey testing as follows. Mice were habituated in von Frey testing boxes for 3 consecutive days, 30min/day. Mechanical thresholds were determined using von Frey filaments according to the Chaplan method.[81,82] Mice were then baselined and injected with 10uL of 50% CFA emulsion into the plantar region of the paw. 24 hours later mice were baselined then injected with 5.6 mg/kg morphine or 5.6 mg/kg compound **38** dissolved in 10% DMSO/10% Cremaphor/80% saline. Time-course taken over 2-hour period. Data analyzed according to Christenzen et al.,[82] and represents the mean ± SEM of the 50% mechanical threshold (n = 6). Statistical analysis performed using nonparametric One-Way ANOVA (Friedman test), Dunn's post-hoc correction. *$p < 0.05$ versus 0 min time point.

ASSOCIATED CONTENT

Supporting Information. The following supporting information files are available

1. AC1 IC_{90}s, cell viability, off-target AC isoform inhibition, PDSP data, opioid receptor data, kinase inhibition and *h*ERG data. (PDF)

2. Dose-response curves for each analog against AC1 and AC8 (PDF)

3. Compound characterization (NMR, MS, HPLC) for each analog (PDF)

AUTHOR INFORMATION

Corresponding Authors

*Correspondence should be addressed to:

Val J. Watts
College of Pharmacy
Purdue University
575 Stadium Mall Dr.
West Lafayette, IN 47907
Email: wattsv@purdue.edu
Phone: (765) 496-3872

Daniel P. Flaherty
College of Pharmacy
Purdue University
575 Stadium Mall Dr.
West Lafayette, IN 47907
Email: dflaher@purdue.edu
Phone: (765) 494-4761

Author Contributions

The manuscript was written through contributions of all authors. All authors have given approval to the final version of the manuscript.

Funding Sources

This work was funded by the Purdue College of Pharmacy (D.P.F and V.J.W.), Purdue Institute for Drug Discovery (D.P.F. and V.J.W.), Richard and Anne Borch Award and the Research Enhancement Award from the Department of Medicinal Chemistry and Molecular Pharmacology, Indiana Clinical and Translational Sciences Institute, National Institute of Neurological Disorders and Stroke (Grant 1R01NS119917, D.P.F and V.J.W) and the National Institute of Mental Health (Grant R21/R33 MH101673, V.J.W.).

Competing Interests and Disclosures

The authors declare no competing interests or financial disclosures with regard to the research.

Publication

This content is an early research output and has not been peer-reviewed at the time of submission

ACKNOWLEDGMENT

The authors would like to acknowledge Dr. Larisa Avramova and Lan Chan for their assistance with screening and analysis.

Ki determinations, receptor binding profiles, agonist and/or antagonist functional data was generously provided by the National Institute of Mental Health's Psychoactive Drug Screening Program, Contract # HHSN-271-2018-00023-C (NIMH PDSP). The NIMH PDSP is Directed by Bryan L. Roth MD, PhD at the University of North Carolina at Chapel Hill and Project Officer Jamie Driscoll at NIMH, Bethesda MD, USA.

REFERENCES

(1) Cooper, D. M. F.; Crossthwaite, A. J. Higher-Order Organization and Regulation of Adenylyl Cyclases. *Trends in Pharmacological Sciences*. 2006. https://doi.org/10.1016/j.tips.2006.06.002.

(2) Dessauer, C. W.; Watts, V. J.; Ostrom, R. S.; Conti, M.; Dove, S.; Seifert, R. Structures and Small Molecule Modulators of Mammalian Adenylyl Cyclases. *Pharmacol. Rev.* **2017**, *69* (2), 96–139. https://doi.org/10.1124/pr.116.013078.

(3) Sadana, R.; Dessauer, C. W. Physiological Roles for G Protein-Regulated Adenylyl Cyclase Isoforms: Insights from Knockout and Overexpression Studies. *NeuroSignals* **2009**, *17* (1), 5–22. https://doi.org/10.1159/000166277.

(4) Choi, E.-J.; Xia, Z.; Storm, D. R. Stimulation of the Type III Olfactory Adenylyl Cyclase by Calcium and Calmodulin. *Biochemistry* **1992**, *31* (28), 6492–6498.

(5) Tang, W.-J.; Gilman, A. G. Type-Specific Regulation of Adenylyl Cyclase by G Protein Beta Gamma Subunits. *Science (80-.).* **1991**, *254* (5037), 1500–1503.

(6) Guillou, J.-L.; Nakata, H.; Cooper, D. M. F. Inhibition by Calcium of Mammalian Adenylyl Cyclases. *J. Biol. Chem.* **1999**, *274* (50), 35539–35545.

(7) Kandel, E. R. The Molecular Biology of Memory Storage: A Dialogue between Genes and Synapses. *Science*. November 2, 2001, pp 1030–1038. https://doi.org/10.1126/science.1067020.

(8) Zhuo, M. Cortical Excitation and Chronic Pain. *Trends in Neurosciences*. Elsevier Current Trends April 1, 2008, pp 199–207. https://doi.org/10.1016/j.tins.2008.01.003.

(9) Defer, N.; Best-Belpomme, M.; Hanoune, J. Tissue Specificity and Physiological Relevance

of Various Isoforms of Adenylyl Cyclase. *American Journal of Physiology - Renal Physiology*. 2000. https://doi.org/10.1152/ajprenal.2000.279.3.f400.

(10) Zhuo, M. Targeting Neuronal Adenylyl Cyclase for the Treatment of Chronic Pain. *Drug Discovery Today*. 2012. https://doi.org/10.1016/j.drudis.2012.01.009.

(11) Cali, J. J.; Zwaagstra, J. C.; Mons, N.; Cooper, D. M. F.; Krupinski, J. Type VIII Adenylyl Cyclase: A Ca2+/Calmodulin-Stimulated Enzyme Expressed in Discrete Regions of Rat Brain. *J. Biol. Chem.* **1994**.

(12) Fagan, K. A.; Mahey, R.; Cooper, D. M. F. Functional Co-Localization of Transfected Ca2+-Stimulable Adenylyl Cyclases with Capacitative Ca2+ Entry Sites. *J. Biol. Chem.* **1996**, *271* (21), 12438–12444. https://doi.org/10.1074/jbc.271.21.12438.

(13) Wei, F.; Qiu, C. S.; Kim, S. J.; Muglia, L.; Maas, J. W.; Pineda, V. V.; Xu, H. M.; Chen, Z. F.; Storm, D. R.; Muglia, L. J.; Zhuo, M. Genetic Elimination of Behavioral Sensitization in Mice Lacking Calmodulin-Stimulated Adenylyl Cyclases. *Neuron* **2002**, *36* (4), 713–726. https://doi.org/10.1016/S0896-6273(02)01019-X.

(14) Wei, F.; Xia, X. M.; Tang, J.; Ao, H.; Ko, S.; Liauw, J.; Qiu, C. S.; Zhuo, M. Calmodulin Regulates Synaptic Plasticity in the Anterior Cingulate Cortex and Behavioral Responses: A Microelectroporation Study in Adult Rodents. *J. Neurosci.* **2003**, *23* (23), 8402–8409. https://doi.org/10.1523/jneurosci.23-23-08402.2003.

(15) Wang, G. Du; Zhuo, M. Synergistic Enhancement of Glutamate-Mediated Responses by Serotonin and Forskolin in Adult Mouse Spinal Dorsal Horn Neurons. *J. Neurophysiol.* **2002**, *87* (2), 732–739. https://doi.org/10.1152/jn.00423.2001.

(16) Descalzi, G.; Kim, S.; Zhuo, M. Presynaptic and Postsynaptic Cortical Mechanisms of Chronic Pain. *Molecular Neurobiology*. Humana Press 2009, pp 253–259.

https://doi.org/10.1007/s12035-009-8085-9.

(17) Vadakkan, K. I.; Wang, H.; Ko, S. W.; Zastepa, E.; Petrovic, M. J.; Sluka, K. A.; Zhuo, M. Genetic Reduction of Chronic Muscle Pain in Mice Lacking Calcium/Calmodulin-Stimulated Adenylyl Cyclases. *Mol. Pain* **2006**, *2*, 1–10. https://doi.org/10.1186/1744-8069-2-7.

(18) Corder, G.; Doolen, S.; Donahue, R. R.; Winter, M. K.; Jutras, B. L.; He, Y.; Hu, X.; Wieskopf, J. S.; Mogil, J. S.; Storm, D. R.; Wang, Z. J.; McCarson, K. E.; Taylor, B. K. Constitutive μ-Opioid Receptor Activity Leads to Long-Term Endogenous Analgesia and Dependence. *Science (80-.).* **2013**, *341* (6152), 1394–1399. https://doi.org/10.1126/science.1239403.

(19) Wong, S. T.; Athos, J.; Figueroa, X. A.; Pineda, V. V.; Schaefer, M. L.; Chavkin, C. C.; Muglia, L. J.; Storm, D. R. Calcium-Stimulated Adenylyl Cyclase Activity Is Critical for Hippocampus-Dependent Long-Term Memory and Late Phase LTP. *Neuron* **1999**, *23* (4), 787–798. https://doi.org/10.1016/S0896-6273(01)80036-2.

(20) Ferguson, G. D.; Storm, D. R. Why Calcium-Stimulated Adenylyl Cyclases? *Physiology*. American Physiological Society 2004, pp 271–276. https://doi.org/10.1152/physiol.00010.2004.

(21) Chen, T.; O'Den, G.; Song, Q.; Koga, K.; Zhang, M. M.; Zhuo, M. Adenylyl Cyclase Subtype 1 Is Essential for Late-Phase Long Term Potentiation and Spatial Propagation of Synaptic Responses in the Anterior Cingulate Cortex of Adult Mice. *Mol. Pain* **2014**, *10* (1). https://doi.org/10.1186/1744-8069-10-65.

(22) Miao, H. H.; Li, X. H.; Chen, Q. Y.; Zhuo, M. Calcium-Stimulated Adenylyl Cyclase Subtype 1 Is Required for Presynaptic Long-Term Potentiation in the Insular Cortex of

Adult Mice. *Mol. Pain* **2019**, *15*. https://doi.org/10.1177/1744806919842961.

(23) Villacres, E. C.; Wong, S. T.; Chavkin, C.; Storm, D. R. Type I Adenylyl Cyclase Mutant Mice Have Impaired Mossy Fiber Long-Term Potentiation. *J. Neurosci.* **1998**, *18* (9), 3186–3194. https://doi.org/10.1523/jneurosci.18-09-03186.1998.

(24) Wei, F.; Vadakkan, K. I.; Toyoda, H.; Wu, L. J.; Zhao, M. G.; Xu, H.; Shum, F. W. F.; Yong, H. J.; Zhuo, M. Calcium Calmodulin-Stimulated Adenylyl Cyclases Contribute to Activation of Extracellular Signal-Regulated Kinase in Spinal Dorsal Horn Neurons in Adult Rats and Mice. *J. Neurosci.* **2006**, *26* (3), 851–861. https://doi.org/10.1523/JNEUROSCI.3292-05.2006.

(25) Shan, Q.; Chan, G. C. K.; Storm, D. R. Type 1 Adenylyl Cyclase Is Essential for Maintenance of Remote Contextual Fear Memory. *J. Neurosci.* **2008**, *28* (48), 12864–12867. https://doi.org/10.1523/JNEUROSCI.2413-08.2008.

(26) Sunahara, R. K.; Taussig, R. Isoforms of Mammalian Adenylyl Cyclase: Multiplicities of Signaling. *Molecular interventions*. 2002. https://doi.org/10.1124/mi.2.3.168.

(27) Avidor-Reiss, T.; Nevo, I.; Saya, D.; Bayewitch, M.; Vogel, Z. Opiate-Induced Adenylyl Cyclase Superactivation Is Isozyme-Specific. *J. Biol. Chem.* **1997**, *272* (8), 5040–5047. https://doi.org/10.1074/jbc.272.8.5040.

(28) Lane-Ladd, S. B.; Pineda, J.; Boundy, V. A.; Pfeuffer, T.; Krupinski, J.; Aghajanian, G. K.; Nestler, E. J. CREB (CAMP Response Element-Binding Protein) in the Locus Coeruleus: Biochemical, Physiological, and Behavioral Evidence for a Role in Opiate Dependence. *J. Neurosci.* **1997**, *17* (20), 7890–7901. https://doi.org/10.1523/jneurosci.17-20-07890.1997.

(29) Algera, M. H.; Kamp, J.; van der Schrier, R.; van Velzen, M.; Niesters, M.; Aarts, L.; Dahan, A.; Olofsen, E. Opioid-Induced Respiratory Depression in Humans: A Review of

Pharmacokinetic–Pharmacodynamic Modelling of Reversal. *British Journal of Anaesthesia*. 2019. https://doi.org/10.1016/j.bja.2018.12.023.

(30) Bateman, J. T.; Levitt, E. S. Evaluation of G Protein Bias and β-Arrestin 2 Signaling in Opioid-Induced Respiratory Depression. American Physiological Society Rockville, MD 2021.

(31) Dahan, A.; Sarton, E.; Teppema, L.; Olievier, C.; Nieuwenhuijs, D.; Matthes, H. W. D.; Kieffer, B. L. Anesthetic Potency and Influence of Morphine and Sevoflurane on Respiration in μ-Opioid Receptor Knockout Mice. *J. Am. Soc. Anesthesiol.* **2001**, *94* (5), 824–832.

(32) Kumar, L.; Barker, C.; Emmanuel, A. Opioid-Induced Constipation: Pathophysiology, Clinical Consequences, and Management. *Gastroenterology Research and Practice*. 2014. https://doi.org/10.1155/2014/141737.

(33) Ma, M.; Li, X.; Tong, K.; Cheng, J.; Yu, Z.; Ren, F.; Zhong, B.; Shi, W. Discovery of Biased Mu-Opioid Receptor Agonists for the Treatment of Pain. *ChemMedChem* **2020**, *15* (1), 155–161. https://doi.org/10.1002/cmdc.201900575.

(34) Brust, T. F.; Alongkronrusmee, D.; Soto-Velasquez, M.; Baldwin, T. A.; Ye, Z.; Dai, M.; Dessauer, C. W.; Van Rijn, R. M.; Watts, V. J. Identification of a Selective Small-Molecule Inhibitor of Type 1 Adenylyl Cyclase Activity with Analgesic Properties. *Sci. Signal.* **2017**, *10* (467). https://doi.org/10.1126/scisignal.aah5381.

(35) Kaur, J.; Soto-Velasquez, M.; Ding, Z.; Ghanbarpour, A.; Lill, M. A.; van Rijn, R. M.; Watts, V. J.; Flaherty, D. P. Optimization of a 1,3,4-Oxadiazole Series for Inhibition of Ca2+/Calmodulin-Stimulated Activity of Adenylyl Cyclases 1 and 8 for the Treatment of Chronic Pain. *Eur. J. Med. Chem.* **2019**, *162*, 568–585.

https://doi.org/10.1016/j.ejmech.2018.11.036.

(36) Wang, H.; Xu, H.; Wu, L. J.; Kim, S. S.; Chen, T.; Koga, K.; Descalzi, G.; Gong, B.; Vadakkan, K. I.; Zhang, X.; Kaang, B. K.; Zhuo, M. Identification of an Adenylyl Cyclase Inhibitor for Treating Neuropathic and Inflammatory Pain. *Sci. Transl. Med.* **2011**, *3* (65). https://doi.org/10.1126/scitranslmed.3001269.

(37) Fain, J. N.; Pointer, R. H.; Ward, W. F. Effects of Adenosine Nucleosides on Adenylate Cyclase, Phosphodiesterase, Cyclic Adenosine Monophosphate Accumulation, and Lipolysis in Fat Cells. *J. Biol. Chem.* **1972**, *247* (21), 6866–6872.

(38) Brand, C. S.; Hocker, H. J.; Gorfe, A. A.; Cavasotto, C. N.; Dessauer, C. W. Isoform Selectivity of Adenylyl Cyclase Inhibitors: Characterization of Known and Novel Compounds. *J. Pharmacol. Exp. Ther.* **2013**. https://doi.org/10.1124/jpet.113.208157.

(39) Denessiouk, K. A.; Rantanen, V.-V.; Johnson, M. S. Adenine Recognition: A Motif Present in ATP-, CoA-, NAD-, NADP-, and FAD-Dependent Proteins. *Proteins Struct. Funct. Genet.* **2001**, *44* (3), 282–291. https://doi.org/10.1002/prot.1093.

(40) Baell, J. B.; Nissink, J. W. M. Seven Year Itch: Pan-Assay Interference Compounds (PAINS) in 2017 - Utility and Limitations. *ACS Chemical Biology*. American Chemical Society January 19, 2018, pp 36–44. https://doi.org/10.1021/acschembio.7b00903.

(41) Baell, J. B.; Holloway, G. a. New Substructure Filters for Removal of Pan Assay Interference Compounds (PAINS) from Screening Libraries and for Their Exclusion in Bioassays. *J. Med. Chem.* **2010**, *53* (7), 2719–2740. https://doi.org/10.1021/jm901137j.

(42) Abdel-Mohsen, H. T.; Conrad, J.; Harms, K.; Nohr, D.; Beifuss, U. Laccase-Catalyzed Green Synthesis and Cytotoxic Activity of Novel Pyrimidobenzothiazoles and Catechol Thioethers. *RSC Adv.* **2017**, *7* (28), 17427–17441. https://doi.org/10.1039/C6RA28102H.

(43) Gu, S. X.; Qiao, H.; Zhu, Y. Y.; Shu, Q. C.; Liu, H.; Ju, X. L.; De Clercq, E.; Balzarini, J.; Pannecouque, C. A Novel Family of Diarylpyrimidines (DAPYs) Featuring a Diatomic Linker: Design, Synthesis and Anti-HIV Activities. *Bioorganic Med. Chem.* **2015**, *23* (20), 6587–6593. https://doi.org/10.1016/j.bmc.2015.09.020.

(44) Kotaiah, S.; Reddy Ramadevi, Dv. B.; Naidu, A.; Dubey, P. K. *SYNTHESIS OF 4-CHLORO-2-(3,5-DIMETHYL-1H-PYRAZOL-1-YL)-6-METHYLPYRIMIDINE*; 2014; Vol. 4.

(45) Patnaik, S.; Basu, D.; Southall, N.; Dehdashti, S.; Wan, K. K.; Zheng, W.; Ferrer, M.; Taylor, M.; Engel, D. A.; Marugan, J. J. Identification, Design and Synthesis of Novel Pyrazolopyridine Influenza Virus Nonstructural Protein 1 Antagonists. *Bioorganic Med. Chem. Lett.* **2019**, *29* (9), 1113–1119. https://doi.org/10.1016/j.bmcl.2019.02.027.

(46) Due-Hansen, M. E.; Pandey, S. K.; Christiansen, E.; Andersen, R.; Hansen, S. V. F.; Ulven, T. A Protocol for Amide Bond Formation with Electron Deficient Amines and Sterically Hindered Substrates. *Org. Biomol. Chem.* **2016**, *14*, 430–433. https://doi.org/10.1039/c5ob02129d.

(47) Bagal, S. K.; Omoto, K.; Blakemore, D. C.; Bungay, P. J.; Bilsland, J. G.; Clarke, P. J.; Corbett, M. S.; Cronin, C. N.; Cui, J. J.; Dias, R.; Flanagan, N. J.; Greasley, S. E.; Grimley, R.; Johnson, E.; Fengas, D.; Kitching, L.; Kraus, M. L.; McAlpine, I.; Nagata, A.; Waldron, G. J.; Warmus, J. S. Discovery of Allosteric, Potent, Subtype Selective, and Peripherally Restricted TrkA Kinase Inhibitors. *J. Med. Chem.* **2019**, *62* (1), 247–265. https://doi.org/10.1021/acs.jmedchem.8b00280.

(48) Soto-Velasquez, M.; Hayes, M. P.; Alpsoy, A.; Dykhuizen, E. C.; Watts, V. J. A Novel CRISPR/Cas9-Based Cellular Model to Explore Adenylyl Cyclase and CAMP Signaling.

Mol. Pharmacol. **2018**, *94* (3), 963–972. https://doi.org/10.1124/mol.118.111849.

(49) Ludwig, M.-G.; Vanek, M.; Guerini, D.; Gasser, J. A.; Jones, C. E.; Junker, U.; Hofstetter, H.; Wolf, R. M.; Seuwen, K. Proton-Sensing G-Protein-Coupled Receptors. *Nature* **2003**, *425* (6953), 93–98.

(50) Zheng, K.; Park, C. M.; Iqbal, S.; Hernandez, P.; Park, H.; LoGrasso, P. V; Feng, Y. Pyridopyrimidinone Derivatives as Potent and Selective C-Jun N-Terminal Kinase (JNK) Inhibitors. *ACS Med. Chem. Lett.* **2015**, *6* (4), 413–418.

(51) Woods, K. W.; Lai, C.; Miyashiro, J. M.; Tong, Y.; Florjancic, A. S.; Han, E. K.; Soni, N.; Shi, Y.; Lasko, L.; Leverson, J. D. Aminopyrimidinone Cdc7 Kinase Inhibitors. *Bioorg. Med. Chem. Lett.* **2012**, *22* (5), 1940–1943.

(52) Bowes, J.; Brown, A. J.; Hamon, J.; Jarolimek, W.; Sridhar, A.; Waldron, G.; Whitebread, S. Reducing Safety-Related Drug Attrition: The Use of in Vitro Pharmacological Profiling. *Nat. Rev. Drug Discov.* **2012**, *11* (12), 909–922. https://doi.org/10.1038/nrd3845.

(53) Tan, H.; Semin, D.; Wacker, M.; Cheetham, J. An Automated Screening Assay for Determination of Aqueous Equilibrium Solubility Enabling SPR Study during Drug Lead Optimization. *JALA - J. Assoc. Lab. Autom.* **2005**, *10* (6), 364–373. https://doi.org/10.1016/j.jala.2005.06.003.

(54) Sou, T.; Bergström, C. A. S. Automated Assays for Thermodynamic (Equilibrium) Solubility Determination. *Drug Discov. Today Technol.* **2018**, *27*, 11–19. https://doi.org/10.1016/j.ddtec.2018.04.004.

(55) Rankovic, Z. CNS Drug Design: Balancing Physicochemical Properties for Optimal Brain Exposure. *J. Med. Chem.* **2015**, *58* (6), 2584–2608. https://doi.org/10.1021/jm501535r.

(56) Hitchcock, S. A.; Pennington, L. D. Structure− Brain Exposure Relationships. *J. Med.*

Chem. **2006**, *49* (26), 7559–7583.

(57) Leeson, P. D.; Davis, A. M. Time-Related Differences in the Physical Property Profiles of Oral Drugs. *J. Med. Chem.* **2004**, *47* (25), 6338–6348.

(58) Wager, T. T.; Chandrasekaran, R. Y.; Hou, X.; Troutman, M. D.; Verhoest, P. R.; Villalobos, A.; Will, Y. Defining Desirable Central Nervous System Drug Space through the Alignment of Molecular Properties, in Vitro ADME, and Safety Attributes. *ACS Chem. Neurosci.* **2010**, *1* (6), 420–434. https://doi.org/10.1021/cn100007x.

(59) Hitchcock, S. A. Structural Modifications That Alter the P-Glycoprotein Efflux Properties of Compounds. *J. Med. Chem.* **2012**, *55* (11), 4877–4895.

(60) Pajouhesh, H.; Lenz, G. R. Medicinal Chemical Properties of Successful Central Nervous System Drugs. *NeuroRx* **2005**, *2* (4), 541–553.

(61) Raub, T. J.; Lutzke, B. S.; Andrus, P. K.; Sawada, G. A.; Staton, B. A. Early Preclinical Evaluation of Brain Exposure in Support of Hit Identification and Lead Optimization. In *Optimizing the "Drug-Like" properties of leads in drug discovery*; Springer, 2006; pp 355–410.

(62) Ghose, A. K.; Herbertz, T.; Hudkins, R. L.; Dorsey, B. D.; Mallamo, J. P. Knowledge-Based, Central Nervous System (CNS) Lead Selection and Lead Optimization for CNS Drug Discovery. *ACS Chem. Neurosci.* **2012**, *3* (1), 50–68. https://doi.org/10.1021/cn200100h.

(63) Avdeef, A.; Deli, M. A.; Neuhaus, W. In Vitro Assays for Assessing BBB Permeability: Artificial Membrane and Cell Culture Models. In *Blood – Brain Barrier in Drug Discovery: Optimizing Brain Exposure of CNS Drugs and Minimizing Brain Side for Peripheral Drugs*; Di, L., Kern, E. H., Eds.; John Wiley & Sons, 2015; pp 188–237.

(64) Lerchner, A.; Machauer, R.; Betschart, C.; Veenstra, S.; Rueeger, H.; McCarthy, C.; Tintelnot-Blomley, M.; Jaton, A.-L.; Rabe, S.; Desrayaud, S. Macrocyclic BACE-1 Inhibitors Acutely Reduce Aβ in Brain after Po Application. *Bioorg. Med. Chem. Lett.* **2010**, *20* (2), 603–607.

(65) Weiss, M. M.; Williamson, T.; Babu-Khan, S.; Bartberger, M. D.; Brown, J.; Chen, K.; Cheng, Y.; Citron, M.; Croghan, M. D.; Dineen, T. A. Design and Preparation of a Potent Series of Hydroxyethylamine Containing β-Secretase Inhibitors That Demonstrate Robust Reduction of Central β-Amyloid. *J. Med. Chem.* **2012**, *55* (21), 9009–9024.

(66) McCoull, W.; Barton, P.; Brown, A. J. H.; Bowker, S. S.; Cameron, J.; Clarke, D. S.; Davies, R. D. M.; Dossetter, A. G.; Ertan, A.; Fenwick, M. Identification, Optimization, and Pharmacology of Acylurea GHS-R1a Inverse Agonists. *J. Med. Chem.* **2014**, *57* (14), 6128–6140.

(67) Pires, D. E. V.; Blundell, T. L.; Ascher, D. B. PkCSM: Predicting Small-Molecule Pharmacokinetic and Toxicity Properties Using Graph-Based Signatures. *J. Med. Chem.* **2015**, 150410113631003. https://doi.org/10.1021/acs.jmedchem.5b00104.

(68) Brändén, G.; Sjögren, T.; Schnecke, V.; Xue, Y. Structure-Based Ligand Design to Overcome CYP Inhibition in Drug Discovery Projects. *Drug Discov. Today* **2014**, *19* (7), 905–911. https://doi.org/10.1016/j.drudis.2014.03.012.

(69) Anzenbacher, P.; Anzenbacherova, E. Cytochromes P450 and Metabolism of Xenobiotics. *Cell. Mol. Life Sci. C.* **2001**, *58* (5), 737–747.

(70) Waring, M. J.; Arrowsmith, J.; Leach, A. R.; Leeson, P. D.; Mandrell, S.; Owen, R. M.; Pairaudeau, G.; Pennie, W. D.; Pickett, S. D.; Wang, J.; Wallace, O.; Weir, A. An Analysis of the Attrition of Drug Candidates from Four Major Pharmaceutical Companies. *Nat. Rev.*

Drug Discov. **2015**, *14*, 475–486. https://doi.org/10.1038/nrd4609.

(71) Ishikawa, M.; Hashimoto, Y. Improvement in Aqueous Solubility in Small Molecule Drug Discovery Programs by Disruption of Molecular Planarity and Symmetry. *J. Med. Chem.* **2011**, *54* (6), 1539–1554. https://doi.org/10.1021/jm101356p.

(72) Papadatos, G.; Alkarouri, M.; Gillet, V. J.; Willett, P.; Kadirkamanathan, V.; Luscombe, C. N.; Bravi, G.; Richmond, N. J.; Pickett, S. D.; Hussain, J.; Pritchard, J. M.; Cooper, A. W. J.; Macdonald, S. J. F. Lead Optimization Using Matched Molecular Pairs: Inclusion of Contextual Information for Enhanced Prediction of HERG Inhibition, Solubility, and Lipophilicity. *J. Chem. Inf. Model.* **2010**, *50* (10), 1872–1886. https://doi.org/10.1021/ci100258p.

(73) Ullah, I.; Gahalawat, S.; Booshehri, L. M.; Niederstrasser, H.; Majumdar, S.; Leija, C.; Bradford, J. M.; Hu, B.; Ready, J. M.; Wetzel, D. M. An Antiparasitic Compound from the Medicines for Malaria Venture Pathogen Box Promotes Leishmania Tubulin Polymerization. *ACS Infect. Dis.* **2020**, *6* (8), 2057–2072.

(74) Besnard, J.; Ruda, G. F.; Setola, V.; Abecassis, K.; Rodriguiz, R. M.; Huang, X.-P.; Norval, S.; Sassano, M. F.; Shin, A. I.; Webster, L. A.; Simeons, F. R.; Stojanovski, L.; PPrat, A.; Seidah, N. G.; Constam, D. B.; Bickerton, R.; Read, K. D.; Wetsel, W. C.; Gilbert, I. H.; Roth, B. L.; Hopkins, A. L. Automated Design of Ligands to Polypharmacological Profiles. *Nature* **2012**, *492* (7428), 215–220.

(75) Kroeze, W. K.; Sassano, M. F.; Huang, X. P.; Lansu, K.; McCorvy, J. D.; Giguère, P. M.; Sciaky, N.; Roth, B. L. PRESTO-Tango as an Open-Source Resource for Interrogation of the Druggable Human GPCRome. *Nat. Struct. Mol. Biol.* **2015**, *22* (5), 362–369. https://doi.org/10.1038/nsmb.3014.

(76) Finlayson, K.; Turnbull, L.; January, C. T.; Sharkey, J.; Kelly, J. S. [3H] Dofetilide Binding to HERG Transfected Membranes: A Potential High Throughput Preclinical Screen. *Eur. J. Pharmacol.* **2001**, *430* (1), 147–148.

(77) Hidalgo, I. J.; Raub, T. J.; Borchardt, R. T. Characterization of the Human Colon Carcinoma Cell Line (Caco-2) as a Model System for Intestinal Epithelial Permeability. *Gastroenterology* **1989**, *96* (2), 736–749.

(78) Kaur, J.; Cao, X.; Abutaleb, N. S.; Elkashif, A.; Graboski, A. L.; Krabill, A. D.; AbdelKhalek, A. H.; An, W.; Bhardwaj, A.; Seleem, M. N.; Flaherty, D. P. Optimization of Acetazolamide-Based Scaffold as Potent Inhibitors of Vancomycin-Resistant Enterococcus. *J. Med. Chem.* **2020**, *63* (17), 9540–9562. https://doi.org/10.1021/acs.jmedchem.0c00734.

(79) Stresser, D. M.; Blanchard, A. P.; Turner, S. D.; Erve, J. C. L.; Dandeneau, A. A.; Miller, V. P.; Crespi, C. L. Substrate-Dependent Modulation of CYP3A4 Catalytic Activity: Analysis of 27 Test Compounds with Four Fluorometric Substrates. *Drug Metab. Dispos.* **2000**, *28* (12), 1440–1448.

(80) Obach, R. S.; Baxter, J. G.; Liston, T. E.; Silber, B. M.; Jones, B. C.; Macintyre, F.; Rance, D. J.; Wastall, P. The Prediction of Human Pharmacokinetic Parameters from Preclinical and in Vitro Metabolism Data. *J. Pharmacol. Exp. Ther.* **1997**, *283* (1), 46–58.

(81) Chaplan, S. R.; Bach, F. W.; Pogrel, J. W.; Chung, J. M.; Yaksh, T. L. Quantitative Assessment of Tactile Allodynia in the Rat Paw. *J. Neurosci. Methods* **1994**, *53* (1), 55–63.

(82) Christensen, S. L.; Hansen, R. B.; Storm, M. A.; Olesen, J.; Hansen, T. F.; Ossipov, M.; Izarzugaza, J. M. G.; Porreca, F.; Kristensen, D. M. Von Frey Testing Revisited: Provision of an Online Algorithm for Improved Accuracy of 50% Thresholds. *Eur. J. Pain* **2020**, *24* (4), 783–790.